25 Edelman
Irvine CA 92618

949.420.3030 phone
530.756.5991 fax
westyost.com

TECHNICAL MEMORANDUM

DATE: October 1, 2026 Project No.: 941-80-26-22

TO: Ground-Level Monitoring Committee (GLMC)
Chino Basin Watermaster

FROM: Lucy Hedley
Eric Chiang, PhD

REVIEWED BY: Andy Malone, PG

SUBJECT: DRAFT: Construction and Calibration of Additional One-Dimensional (1D) Compaction Models in the Western Portion of the Chino Basin

BACKGROUND AND OBJECTIVES

Pursuant to the Peace Agreement[1], the Chino Basin Watermaster developed an adaptive Subsidence Management Plan (SMP)[2], which provides guidance for groundwater management to minimize or abate the future occurrence of land subsidence within the Chino Basin. The SMP identifies several "Areas of Subsidence Concern" across the western portion of Chino Basin where the future occurrence of land subsidence and ground fissuring is a concern. Figure 1 is a map that shows the location of these areas (outlined in green), which were identified based on the following observations:

- The underlying hydrogeologic conditions, particularly the numerous fine-grained interbeds and clay layers within the aquifer system (aquitards), are susceptible to aquifer-system compaction and associated land subsidence.
- Land subsidence is occurring in these areas or has occurred in the recent past.
- Historical declines in groundwater levels in these areas since the early- to mid-1900s were extreme (>150 feet) and could still be causing the current land subsidence due to delayed drainage of aquitards.

[1] Section 1.1 (y) of the Peace Agreement.

[2] Wildermuth Environmental, Inc. 2015. Chino Basin Subsidence Management Plan. Prepared for the Chino Basin Watermaster. July 23, 2015.

- Conditions that are conducive to ground fissuring are present, such as geologic faults that act as groundwater barriers which can lead to differential subsidence.
- Increases in groundwater pumping (and associated declines in hydraulic heads) are occurring or are planned to occur within or near these areas.

The SMP also calls for the use of computer-simulation modeling to assist in subsidence management efforts and future updates to the SMP. One-dimensional compaction models can simulate the process of aquitard drainage and compression/compaction using an aquitard-drainage model. This model describes how head decline in a coarse-grained aquifer causes the gradual drainage of pore water from the clay interbeds within aquifers and the confining layers separating them, resulting in compression and/or permanent compaction of the clay interbeds. In a 1D compaction model, the time-series of head in the coarser-grained aquifer sediments is assumed to be known, either from physical measurements or groundwater model simulations. The 1D model then solves for the gradual drainage of the clay layers and calculates the resulting compression/compaction. Since 1D models simulate one location in a groundwater basin through the entire thickness of the aquifer system, they can be constructed at high depth resolution, which gives them the ability to simulate both compaction in multilayered aquifer systems and the residual compaction of thicker clay layers within the aquifers.

To date, two 1D models have been constructed and calibrated in the Chino Basin in Northwest MZ-1. These two models were developed to assess acute areas of subsidence in the Northwest MZ-1 area and to support the development of a *Subsidence Management Plan for Northwest MZ-1.*[3] The objective of the plan is to provide guidance for the Watermaster and the Parties for how to manage hydraulic heads in Northwest MZ-1 (potentially through the management of pumping, recharge, the use of managed storage, and/or the design and implementation of Storage and Recovery Programs) so that the future occurrence of subsidence is minimized or abated in this area. Figure 1 shows the location of these two 1D models (and the Watermaster's current ground-level monitoring network):

- **MVWD-28**. This 1D model was constructed and calibrated in Northwest MZ-1 in 2017.[4] The model was constructed using the borehole lithology and geophysical data from Monte Vista Water District (MVWD) Well 28.

[3] Wildermuth Environmental, Inc. 2015. Work Plan to Develop a Subsidence-Management Plan for Northwest MZ-1. Prepared for the Chino Basin Watermaster. July 23, 2015.

[4] Wildermuth Environmental, Inc. 2017. *Task 3 and Task 4 of the Work Plan to Develop a Subsidence Management Plan for the Northwest MZ-1 Area: Development and Evaluation of Baseline and Initial Subsidence-Management Alternatives*. Prepared for Ground-Level Monitoring Committee, Chino Basin Watermaster. December 13, 2017.

- **PX**. This 1D model was constructed and calibrated in Northwest MZ-1 in 2022.[5] The model was constructed using the borehole lithology and geophysical data from the deep borehole at the Pomona Extensometer (PX).

Both 1D models were calibrated using piezometric data, model estimates for historical heads, ground-level survey data at nearby benchmarks, and InSAR estimates of vertical ground motion. The 1D models were used for the following reasons: to help understand the history of land subsidence in Northwest MZ-1; to help understand the mechanisms behind the subsidence; and to evaluate the potential for aquifer-system compaction within Northwest MZ-1 under future planning scenarios of pumping and recharge.

In 2023, with input from the GLMC, the Watermaster Board approved a scope of work to construct and calibrate three additional 1D models across the other Areas of Subsidence Concern for the following purposes:

- To evaluate for subsidence-related Material Physical Injury (MPI) during future Safe Yield resets (as well as other future MPI evaluations as they arise).
- Inform future updates to the SMP.

In 2024, the GLMC reviewed and commented on a technical memorandum[6] that described the methods and data to be used in the construction and calibration of these three additional 1D models. Figure 1 shows the locations of the three additional 1D models:

- **ONT-33**. This 1D model is located at City of Ontario Well 33 (ONT-33). This location was chosen because gradual and persistent land subsidence has occurred across this area (Northeast Area of Subsidence Concern) since at least 1992, totaling over one foot at this location.
- **CCX**. This 1D model is located at the Chino Creek Extensometer (CCX). This location was chosen because of its proximity to the western portion of the Chino Basin Desalter Authority (CDA) well field, where increased CDA pumping is occurring.
- **APX**. This 1D model is located at the Ayala Park Extensometer (APX). This location was chosen because: the area experience over two feet of land subsidence in the late-1980s and early 1990s; the land subsidence was accompanied by ground fissuring and damage to overlying infrastructure; and the Managed Area is the primary focus of the SMP.

---

[5] West Yost. 2022. *Construction and Calibration of One-Dimensional Compaction Models in the Northwest MZ-1 Area of the Chino Basin*. Prepared for Ground-Level Monitoring Committee, Chino Basin Watermaster. November 22, 2022.

[6] West Yost. 2024. *Proposed Locations and Data for Construction/Calibration of Additional 1D Models*. Prepared for Ground-Level Monitoring Committee, Chino Basin Watermaster. April 24, 2024.

The main objective of this technical memorandum is to describe the methods for and the results of the construction and calibration of the three additional 1D models. Ancillary objectives are to describe the subsidence mechanisms and the vertical distribution of pre-consolidation head[7] within the aquifer system across the western portion of Chino Basin. Knowledge of the subsidence mechanisms and pre-consolidation heads can provide guidance for the Chino Basin parties in the development of subsidence-management strategies (i.e., managed pumping and/or recharge) to avoid the future occurrence of adverse impacts associated with land subsidence.

METHODS AND DATA

This section describes:

- Background information on the modeling tools used to estimate head changes and aquifer system deformation.
- The technical methods and data that were used to construct and calibrate the three additional 1D models in western Chino Basin.

Model Codes Used

The United States Geological Survey (USGS) has developed a wide range of computer models to simulate saturated and unsaturated subsurface flow, solute transport, and chemical reactions in groundwater systems. The most widely used of these models is MODFLOW, which simulates three-dimensional (3D) groundwater flow using the finite-difference method. Although it was conceived solely as a groundwater flow model in 1984 and released in 1988 (McDonald et al., 1988), the MODFLOW modular structure has provided a robust framework for the integration of additional simulation capabilities that build on and enhance its original scope. The family of MODFLOW-related models now includes capabilities for simulating coupled groundwater/surface water systems and solute transport.

MODFLOW-NWT (Niswonger et al., 2011) was chosen for this project because: 1) it has extensive publicly available documentation, 2) it has sustained rigorous USGS and academic peer review, 3) it has a long history of development and use, 4) it is widely used around the world in public and private sectors, 5) it can easily operate with additional simulation tools published by others, and 6) it has been used by the Watermaster in the 2020 Chino Valley Model (2020 CVM) for the 2020 Safe Yield Recalculation (WEI, 2020) and for the 1D Models developed for Northwest MZ-1.

The Interbed Storage Package (Leake and others, 1991) of MODFLOW-NWT was chosen to simulate the aquifer-system deformation that is caused by elastic and/or inelastic deformation of

[7] The pre-consolidation head is the lowest piezometric level that an aquifer system has ever experienced. When piezometric levels are below the pre-consolidation head, permanent subsidence is caused.

the fine-grained interbeds in an aquifer-system due to changes in the effective stress on the soil skeleton because of changing groundwater levels.

How MODFLOW Works

In a MODFLOW model, an aquifer system is represented by a discretized domain consisting of an array of finite difference blocks (model cells) and nodes at the cell centers. The figure below shows the spatial discretization scheme of an aquifer system with a mesh of model cells and nodes at which hydraulic heads are calculated.[8] Hydrostratigraphic units can be represented by one or more model layers and the layer of thickness may vary from cell to cell. The nodal grid forms the framework of a finite-difference numerical model.

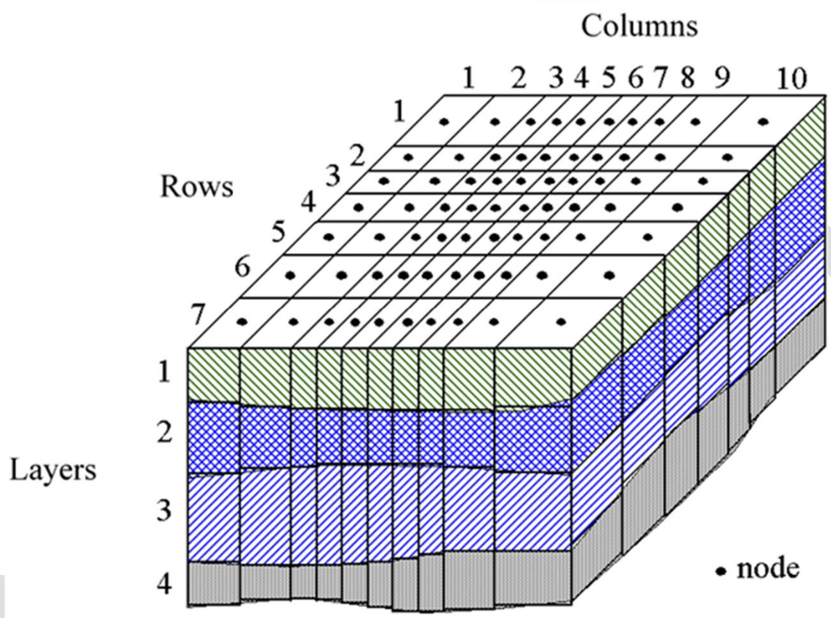

Spatial discretization scheme of MODFLOW

To calculate the hydraulic heads at the nodes (i.e., centers of model cells), a water balance equation is formulated for each model cell:

$$\Sigma Q = S_s \cdot \frac{\Delta h}{\Delta t} \cdot V + S' \cdot \frac{\Delta h}{\Delta t} \qquad (1)$$

The left-hand side of the equation (ΣQ) is the sum of all flows to/from neighboring cells, pumping, and recharge occurring within the model cell. The right-hand side represents the storage change within a time-interval of the length Δt, where Ss is the specific storage (that accounts for compressibility of water), S’ is the Skeletal storage coefficient (that accounts for compressibility

[8] Wróbel, Michał, Brandyk, Andrzej & Tereba, Anna. (2023). *Modflow model in the assessment of water conditions in forest areas*. International Journal of Hydrology Science and Technology. 15. 207. 10.1504/IJHST.2023.130080.

of soil skeleton) of the model cell, V is the volume of the model cell, and $\Delta \mathrm{h}$ is the head change in the model cell over the time interval Δt. The flows to/from neighboring cells can be expressed with the hydraulic heads of the model cell and its neighbors through the Darcy's law that describes the relationship between the flow, hydraulic conductivity, and hydraulic gradient. In summary, equation (1) can be rewritten to an equation containing unknown hydraulic head values at the cell and its neighboring cells with other aquifer property terms.

MODFLOW formulates such an equation for each of the active model cells (where the heads are unknown and need to be solved). Once all equations are formulated, the system of equations are solved together for the unknown head values. Once the head values are computed, they are used to back-calculate the cell-by-cell flow terms. The calculated head values and flow terms are the basis for water budget calculation, particle tracking simulations, transport models, and visualization, such as flow vectors and water level contours.

Estimating the Vertical Aquifer-System Deformation in a Model Cell

The vertical deformation of a model cell (Δb) over a time interval Δt is calculated as:

$$\Delta \mathrm{b} = S' \cdot \Delta h \qquad (2)$$

Soil skeleton deformation behavior is non-linear and is dependent on the current hydraulic head and the lowest hydraulic head (i.e., highest effective stress) that has ever been applied to the soil skeleton. To better approximate the non-linear behavior, equation (2) is further refined as follows:

$$\Delta \mathrm{b}_e = S_{fe} \cdot \Delta h \qquad if\ h > h_c \qquad (3a)$$

$$\Delta \mathrm{b}_v = S_{fv} \cdot \Delta h \qquad if\ h \le h_c \qquad (3b)$$

The variable h_c is the pre-consolidation head (also referred to as critical head, or the previous lowest hydraulic head) of the model cell; $\Delta \mathrm{b}_e$ is the elastic deformation; S_{fe} is the elastic storage coefficient; $\Delta \mathrm{b}_v$ is the inelastic deformation; and S_{fv} is the inelastic storage coefficient. Equation (3a) applies when the hydraulic head is greater than the pre-consolidation head. Equation (3b) applies when the hydraulic head is equal or less than the pre-consolidation head.

If the hydraulic head remains greater than the pre-consolidation head, a further decrease in hydraulic head (i.e., increase in effective stress) causes a small elastic compression in both the coarse- and fine-grained sediments. This compression is recoverable if the head returns to its initial value. If the hydraulic head falls below the pre-consolidation head, the fine-grained sediments can compact inelastically. Inelastic compaction is explained by a physical rearrangement of the sediment grains and is largely permanent (Meade, 1964). Inelastic compaction of coarse-grained sediments is generally negligible compared to that of fine-grained sediments. For the same magnitude of changes in effective stress, inelastic compaction can be one to two orders of magnitude larger than elastic compression (Riley, 1969; Riley 1998).

Time Delay of Compaction

Because of the characteristically low vertical hydraulic conductivity of fine-grained interbeds, the equilibration of hydraulic heads in the interbeds of an aquifer system typically lags the head changes in the bounding aquifers (Hoffmann and others, 2003). In the context of interbed compaction and land subsidence, the time delay caused by slow dissipation of transient overpressures in fine-grained interbed sediments is often given in terms of the time constant τ_0.

$$\tau_0 = \left(\frac{b_0}{2}\right)^2 / D' \quad (4)$$

The time constant τ_0 is the time during which about 93 percent of the ultimate compaction for a given decrease in head occurs (Hoffmann and others, 2003) if the overpressures dissipate vertically in two directions into the bounding aquifers. The variable b_0 is the thickness of the interbed within a model cell and $D' = VK'_v / S'_s$ is the ratio of the vertical hydraulic conductivity (VK'_v) and the specific storage (S'_s) of the interbed. If the time constant τ_0 is significantly greater than the model time steps, the process of slow dissipation of the heads in the interbed must be explicitly simulated (Hoffmann and others, 2003). For most regional 3D groundwater models with large interbed thickness within model layers (such as CVM), the time constant τ_0 is often much greater than the model time steps. The Subsidence and Aquifer Compaction (SUB) Package introduces an approximation method to simulate the slow dissipation of heads in such models, where all interbeds within a model cell (of greater thickness) are lumped together and their root mean square of the thicknesses is used in the simulation. While this method is theoretically sound, it is impractical to accurately collect details of all interbed data for deep aquifers of a 3D model.

To address this challenge, this work used a combination of 3D and 1D models. In this approach, a 3D model is used to simulate regional groundwater head without the skeleton compression (i.e., compaction) terms. A vertical 1D model at a desired location with detailed lithological log is constructed with much higher vertical resolution, where thickness of each model cell is much smaller than the 3D model to obtain a proper time constant τ_0 for given time step lengths. The simulated heads from the 3D model are then assigned as the prescribed heads for the 1D model cells with coarse-grained sediments, and the 1D model run is executed to calculate the vertical aquifer-system deformation within the model cells of fine-grained sediments. The detailed steps of this approach are given below.

Data Used for 1D Model Construction and Calibration

All three 1D models were constructed and calibrated using existing data and information, as summarized below:

ONT-33

Figure 2a shows the lithologic and borehole resistivity data from ONT-33, which was used to construct the 1D model along with the depth intervals of the five layers of the Chino Valley Model (CVM). The lithologic and resistivity data span the depth interval from 0 to about 1,200 feet below ground surface (ft-bgs). These data are sufficient to construct a 1D model that can simulate aquifer-system compaction across the entire thickness of the Chino Basin aquifer system at this location.

Figure 3a shows the time-series data that were used during calibration of the ONT-33 1D model. These data include:

- *Hydraulic Head*. These data were derived from: (i) historical measurements of groundwater elevation at several nearby wells; (ii) estimates of hydraulic head by CVM model layer that were derived from the 2020 CVM calibration (extended through 2022); and (iii) professional judgment.
- *Vertical Ground Motion.* These data were derived from InSAR estimates of vertical ground motion at the ONT-33 location from 1992-2022.

CCX

Figure 2b shows the lithologic and borehole resistivity data from the deep borehole at the CCX, which was used to construct the 1D model along with the depth intervals of the five layers of the CVM. The lithologic and resistivity data span the depth interval from 0 to about 635 ft-bgs. These data are sufficient to construct a 1D model that can simulate aquifer-system compaction across the entire thickness of the Chino Basin aquifer system at this location.

Figure 3b shows the time-series data that were used during calibration of the CCX 1D model. These data include:

- *Hydraulic Head*. These data were derived from: (i) historical measurements of groundwater elevation at several nearby wells; (ii) estimates of hydraulic head by CVM model layer that were derived from the 2020 CVM calibration (extended through 2022); and (iii) professional judgment.
- *Vertical Ground Motion*. These data were derived from: (i) InSAR estimates of vertical ground motion at the CCX location from 2011-2022; (ii) CCX extensometer data; and (iii) traditional leveling surveys at nearby benchmarks.

APX

Figure 2c shows the lithologic and borehole resistivity data from the deep borehole at the Ayala Park Extensometer, which were used to construct the 1D model along with the depth intervals of the five layers of the CVM. The lithologic and resistivity data span the depth interval from 0 to about 1,400 ft-bgs. These data are sufficient to construct a 1D model that can simulate aquifer-system compaction across the entire thickness of the Chino Basin aquifer system at this location.

Figure 3c shows the time-series data that were used during calibration of the CCX 1D model. These data include:

- *Hydraulic Head*. These data were derived from: (i) historical measurements of groundwater elevation at several nearby wells; (ii) estimates of hydraulic head by CVM model layer that were derived from the 2020 CVM calibration (extended through 2022); and (iii) professional judgment.
- *Vertical Ground Motion*. These data were derived from: (i) InSAR estimates of vertical ground motion at the APX location from 1992-1993 and 2005-2022; (ii) Ayala Park extensometer data; and (iii) traditional leveling surveys at nearby benchmarks.

Steps to Construct and Calibrate the 1D Compaction Models

In summary, the major steps to construct and calibrate the 1D models were:

1. Construct the 1D models using the Interbed Storage Package (Leake and others, 1991) of MODFLOW-NWT at areas of maximum historical subsidence. These models are a vertical stack of cells that represent the aquifer system at each location. The thicknesses of the 1D model cells are chosen to ensure that the time constant τ_0 is smaller than model time steps. The model cells are categorized into either “Sand” for coarse-grained sediments or “Clay” for fine-grained sediments based on borehole lithologic and geophysical data. Initial aquifer (Sand) and aquitard (Clay) properties were assigned to the 1D model cells.
2. Prepare a monthly time-series of historical heads by aquifer-system layer to serve as input data for the 1D models over the calibration period. For 1930-1977, these heads are estimated based on the measured groundwater elevations at wells in the vicinity of the 1D models. For 1977-2022, these heads are estimated from 2020 CVM output data for heads at the 1D model locations by model layer. The heads are assigned as prescribed heads to the corresponding Sand cells in the 1D model.
3. Run and calibrate the 1D models over a historical period by adjusting the aquifer and aquitard properties. The 1D model simulations were executed to compute a time series of vertical aquifer-system deformation in each 1D model cell. During calibration, candidate parameter sets were evaluated using both visual comparison and a weighted statistical framework to best match historical observations of land subsidence with model-simulated compaction of the aquifer system. The sum of the calculated vertical deformation in all 1D model cells is assumed to represent the vertical ground motion at the land surface.

RESULTS

This section describes the results of the construction and calibration of the three new 1D models: ONT-33, CCX, and APX.

1D Model Construction and Setup

Figures 2a-c display the borehole lithology at the ONT-33, CCX, and APX sites, which consists of interbedded coarse-grained "Sand" layers comprised of silty sands, sands, and gravels with fine-grained "Clay" layers comprised of silts, silty clays, and clays.[9] Table 1 below shows how the Unified Soils Classification System (USCS) was used to assign borehole lithology descriptions to "Sand" or "Clay" 1D model cell types.

Table 1. Mapping of USCS Codes to "Sand" or "Clay" 1D Model Cells

USCS Code	Description	1D Model Cell Type
SP-SM	Poorly graded sand with silt	Sand
SP-SC	Poorly graded sand with clay	Sand
SP	Poorly graded sand with gravel	Sand
SC	Clayey sand or sand with clay	Sand
SM	Silty sand	Sand
CH	Fat clay	Clay
ML	Sandy silt	Clay
CL	Sandy lean clay or clay with sand	Clay

Figures 2a-c show the results of this mapping for each 1D model (Sand cells are shaded in gray; Clay cells are shaded white) and the corresponding CVM layers. CVM Layer 1 represents the shallow aquifer-system and is generally characterized by unconfined to semi-confined groundwater conditions. CVM Layers 2 to 5 represent the aquifers and aquitards that comprise the deep aquifer-system and are characterized by confined groundwater conditions, lower permeability sand and gravel layers (compared to Layer 1), and a greater abundance of interbedded fine-grained sediments.

The three 1D models were constructed using the same discretization approach. For each 1D model, the subsurface was discretized into a stacked column of one-foot-thick model cells extending from ground surface to the approximate depth of the borehole. Each model cell was

[9] The Ontario Well 33 and the CCX and APX extensometers borehole lithologic and geophysical logs are included in Appendix A to this memorandum.

mapped to the borehole lithology and classified as either "Sand" or "Clay" based on the mapping shown in Table 1. Each model cell was also mapped to one of the five CVM layers based on the CVM Layer configuration at the 1D model location.

Initial Aquifer/Aquitard Properties

Table 2 lists the initial estimates for vertical hydraulic conductivity (VK), specific storage (Ss), and the inelastic and elastic storage coefficients (Sfv and Sfe, respectively) that were assigned to all Sand and Clay cells in all three 1D models. These initial estimates were obtained based on literature reviews and were adjusted during calibration.

Table 2. Initial Aquifer/Aquitard Properties

Cell Type	Aquifer/Aquitard Property	Initial Value
Sand	Vertical hydraulic conductivity (VK)	5.00E-01 [ft/day]
Sand	Specific storage (Ss)	1.83E-06 [1/ft]
Sand	Inelastic storage coefficient (Sfv)	1.00E-06 [-]
Sand	Elastic storage coefficient (Sfe)	1.00E-06 [-]
Clay	Vertical hydraulic conductivity (VK)	2.50E-05 [ft/day]
Clay	Specific storage (Ss)	1.14E-05 [1/ft]
Clay	Inelastic storage coefficient (Sfv)	1.65E-04[-]
Clay	Elastic storage coefficient (Sfe)	4.50E-06 [-]

Initial Conditions

The 1D models required assignment of initial conditions for head, pre-consolidation head, and compaction for each model cell. Initial heads were estimated based on measured groundwater levels at wells located in the vicinity of each 1D model in 1930 and were assigned uniformly to all model cells. The initial pre-consolidation heads were assumed to be equal to the initial heads based on the assumption that significant groundwater-level declines and associated aquifer-system compaction had not occurred by 1930. The following initial head and pre-consolidation head values were assigned.

- ONT-33: 718.1 feet above mean sea level (ft amsl)
- CCX: 591.3 ft amsl
- APX: 632.3 ft amsl

Initial compaction was set to zero for all model cells.

Boundary Conditions

Sand cells in the 1D models were represented as specified-head boundaries using the Flow and Head Boundary Package (Leake and others, 1997).

Figures 3a-c show the head time series assigned to Sand cells in the ONT-33, CCX, and APX 1D models based on the CVM layer to which each Sand cell was mapped. Head time series are shown for CVM Layers 1, 3, and 5. Layers 2 and 4 are not shown because they are composed primarily of Clay cells. Historical heads measured at wells in the vicinity of each model are also shown in Figures 3a-c for comparison.

For the period 1930-1977, measured heads at nearby wells were used to estimate the head time series assigned to the 1D model cells. During this period, virtually all existing pumping wells were screened only in CVM Layer 1. In the absence of measured head data for the deeper layers, heads assigned to Sand cells mapped to CVM Layers 3 and 5 were assumed to decline concurrently with the heads in Layer 1.

For the period 1977-2022, heads simulated by the 2020 CVM at each 1D model location were used to define the head time series assigned to Sand cells based on their mapped CVM layer. This period corresponds to the calibration period of the 2020 CVM. During this period, deeper pumping wells were constructed in all three areas, and head declines occurred in the deeper, confined CVM layers.

Time Discretization

The 1D models were run from August 1, 1930 to July 1, 2022 on a monthly time step.

1D Model Calibration

The calibration of the 1D models was performed in a manual and iterative manner in the following steps:

1. The initial aquifer/aquitard properties for the Sand and Clay cells were assigned to the 1D models.
2. The 1D models were executed from 1930 to 2022 using the prescribed heads by model layer in Figures 3a-c as boundary conditions for the Sand cells in the 1D models.
3. The model-simulated compaction in the Clay cells were summed and compared against the vertical ground motion data (i.e., InSAR, benchmark, and/or extensometer data) over the simulation period, and the goodness of fit was determined via visual and statistical methods.
4. Based on the results of step 3, a new set of aquitard properties for the Clay[10] cells were developed, and steps 1 to 3 were repeated as a new calibration iteration.

The initial aquitard properties in Table 2 were used in calibration iteration V0, and then manually adjusted in subsequent calibration iterations. The iterative calibration process was repeated until a

[10] The potential for compaction in the Sand cells was assumed to be negligible, hence, the aquifer properties for the Sand cells were set to their initial values in Table 2 and were not adjusted during 1D Model calibration.

good match between model-simulated aquifer-system deformation and vertical ground motion were achieved with aquitard properties within reasonable bounds. Tables 3a-c list the aquitard properties for the Clay cells for all calibration iterations for each 1D model.

For the statistical evaluation of goodness-of-fit between observed vertical ground motion and simulated aquifer-system deformation, the observed datasets were combined using a weighted statistical framework. Individual observations were assigned weights based on both dataset type and the number of observations within each dataset. Dataset-type weights were applied to ensure that selected monitoring data sources contributed proportionally to the calibration objectives for each model location. Within each dataset type, the total assigned weight was distributed equally among datasets and then normalized by the number of observations to prevent datasets with larger sample sizes from disproportionately influencing the statistical results. Model performance was assessed using statistical evaluation metrics including the coefficient of determination (R^2), root mean square deviation (RMSD), and Nash-Sutcliffe Efficiency (NSE). Table 4 lists the calibration statistics for all calibration iterations.

For the visual evaluation of goodness-of-fit between observed vertical ground motion and simulated aquifer-system deformation, time-series charts were prepared on Figures 4a-c for the main calibration iterations for each 1D model.

Based on analysis of the calibration statistics and the time-series charts:

- The aquitard properties in calibration iteration **V7** of the ONT-33 1D Model provided the best overall match between the simulated aquifer-system deformation and the InSAR data. See Figure 5a for a more detailed comparison of observed versus simulated.
- The aquitard properties in calibration iteration **V5** of the CCX 1D Model provided the best overall match between the simulated aquifer-system deformation and the observed benchmark and InSAR data. See Figure 5b for a more detailed comparison of observed versus simulated.
- The aquitard properties in calibration iteration **V33** of the APX 1D model provided the best overall match between the simulated aquifer-system deformation and the observed benchmark, InSAR, and extensometer data. See Figure 5c for a more detailed comparison of observed versus simulated.

The final calibrated aquitard properties for all three 1D models are listed below in Table 5. Differences in calibrated aquitard properties between the three models are interpreted to reflect local variations in the texture, composition, age, and consolidation of the fine-grained sediments. The calibrated aquitard properties should not be interpreted as unique but rather as one reasonable set of parameters capable of reproducing the observed deformation behavior.

Table 5. Final Calibrated Aquitard Properties for the Clay Cells in the 1D Models

1D Model	Iteration	VK [ft/day]	Ss [1/ft]	Sfv [-]	Sfe [-]
ONT-33	V7	1.50E-06	3.00E-05	2.00E-04	4.50E-06
CCX	V5	2.50E-05	3.00E-05	1.20E-04	4.50E-06
APX	V33	1.55E-06	5.00E-06	4.50E-05	3.00E-07

RECOMMENDATIONS

The Watermaster Engineer judges the three new 1D models sufficiently calibrated to use in future efforts to evaluate for potential MPI associated with land subsidence. Such evaluations may occur in future Safe Yield resets or other Watermaster efforts of proposed groundwater management actions (e.g., applications for storage and recovery programs).

That said, these are first-generation 1D models that can be improved in the future through model recalibration. Continued monitoring and enhanced understanding of hydrogeologic conditions are crucial to minimizing model error and uncertainty. Specifically, new monitoring information should be used for future 1D model updates and recalibrations, if recommended by the GLMC, including:

- Improved InSAR-derived deformation datasets processed using updated correction and filtering techniques to reduce the influence of atmospheric artifacts, decorrelation, reference-point uncertainty, and localized measurement noise, thereby providing a more accurate estimate of long-term vertical ground motion.
- Additional extensometer data captured at the CCX and APX extensometers, which provide high frequency data at the new 1D model locations.
- Additional ground-level survey and repeated GPS elevation data at monitoring sites near the new 1D model locations.
- Additional groundwater-level data at wells located near the new 1D model locations.

More data of vertical ground motion and depth-specific groundwater levels will allow for improved 1D model calibration and will increase confidence in using the model outputs for subsidence management efforts and as a tool for evaluating subsidence-related MPI.

ANCILLARY UNDERSTANDING OF SUBSIDENCE FROM 1D MODEL CALIBRATION

This section describes ancillary information derived from the final 1D model calibrations, including the estimates of historical subsidence, the mechanisms driving the historical subsidence, and the vertical distribution of critical head within the aquifer system at each 1D model location. This information can provide guidance for the Chino Basin Parties to avoid the future occurrence of land subsidence as described below for each 1D model location.

ONT-33

Figure 6a displays the estimated time history of (i) changes in heads by aquifer layer and (ii) the associated compaction of the aquifer system at ONT-33. The historical time series of InSAR has shown that land subsidence occurred in similar patterns and rates across the Northeast Area, which suggests that Figure 6a is generally representative of the Northeast Area. The following observations and interpretations are made from Figure 6a:

- From 1930 to the mid-1970s, pumping-induced overdraft of the Chino Basin caused over 100 ft of head declines in all three aquifer layers, which in turn, caused about 8 ft of permanent compaction of the aquifer system (and the same magnitude of land subsidence). Compaction was greatest in Layer 1 (about 4 ft).
- From the mid-1970s to 2000, heads generally stabilized in Layers 1 and 3 but pumping from newer deep wells caused another 40 feet of head decline in Layer 5, which in turn, caused about 3 ft of additional permanent compaction of the aquifer system (and the same magnitude of land subsidence). During this period, compaction was greatest in Layer 5 as heads in Layer 5 progressively reached all-time lows.
- From 2000 to 2022, heads in all three aquifer layers increased, particularly within Layer 5, which in turn caused the rates of compaction (and subsidence) to slow considerably. Only about 0.5 ft of compaction occurred during this period, which is interpreted to be "residual" compaction as the pore pressures within the thicker aquitard layers were continuing to equilibrate with the long-term historical head declines that occurred prior to 2000.

Figure 6b displays the vertical distribution of compaction and critical head by aquitard layer at the end of 1D model calibration (June 2022). The following observations and interpretations are made from Figure 6b:

- Critical heads are highest within the central portions of the thickest aquitards, which indicates that pore pressures within the thicker aquitards have only partially equilibrated with the historical head declines in the adjacent aquifer layers, and hence, have only partially compacted.
- The highest critical heads within the aquitard layers are:
    - About 635 ft-amsl in Layers 1, 2 and 3
    - About 600 ft-amsl in Layers 4 and 5
- Additional compaction of the aquitard layers will occur when heads in the aquifers are below the highest critical heads in the aquitards.

- The recent observations of relatively slow rates of subsidence in the Northeast Area are likely being caused by heads in the aquifers that are slightly lower than the highest critical heads within a few of the thicker aquitards.

CCX

Figure 7a displays the estimated time history of (i) changes in heads by aquifer layer and (ii) the associated compaction of the aquifer system at CCX. The historical time series of InSAR has shown that land subsidence occurred in similar patterns and rates across the Southeast Area, which suggests that Figure 7a is generally representative of the Southeast Area. The following observations and interpretations are made from Figure 7a:

- From 1930 to the late-1970s, pumping-induced overdraft of the Chino Basin caused about 60-80 ft of head declines in all three aquifer layers, which in turn, caused about 2 ft of permanent compaction of the aquifer system (and the same magnitude of land subsidence). The compaction occurred equally in Layers 1 and 3. Compaction in Layer 5 is close to zero because Layer 5 is virtually absent at the CCX location, which is partly responsible for the lesser magnitude of total subsidence at this location compared to the ONT-33 location.
- From the late-1970s to the late-1990s, heads in Layers 1 and 3 stabilized with seasonal fluctuations due to seasonal pumping patterns, which in turn, caused a significant slowing of the rate of compaction.
- From the late-1990s to 2022, heads in Layer 1 increased by about 40 ft due to decreases in agricultural pumping as urban land uses replace agriculture, which in turn caused compaction in Layer 1 to cease. However, heads in Layer 3 declined by about 50 ft through 2016 due to deeper pumping at the nearby CDA well field, which caused about 0.75 ft of additional compaction in Layer 3.
- From 2016-2022, the deeper pumping at the CDA well field ceased due to water quality concerns, heads in Layer 3 increased by about 50 ft, and compaction has virtually ceased at the CCX location.

Figure 7b displays the vertical distribution of compaction and critical head by aquitard layer at the end of 1D model calibration (June 2022). The following observations and interpretations are made from Figure 7b:

- Critical heads within the aquitards are at about 500 ft-amsl and are nearly identical to critical heads in the aquifers, which indicates that pore pressures within the aquitards have nearly equilibrated with the historical head declines in the adjacent aquifer layers.
- Additional compaction of the aquitard layers will only occur when heads in the aquifers decline below about 500 ft-amsl (i.e., the highest critical heads in the aquitards). In

2022, heads within Layers 1 and 3 were at about 550-560 ft-amsl, which is significantly higher than the critical heads in the aquitards.

APX

Figure 8a displays the estimated time history of (i) changes in heads by aquifer layer and (ii) the associated compaction of the aquifer system at APX. The historical time series of InSAR has shown that land subsidence occurred in similar patterns and rates across the Managed Area, which suggests that Figure 8a is generally representative of the Managed Area. The following observations and interpretations are made from Figure 8a:

- From 1930 to the late-1970s, pumping-induced overdraft of the Chino Basin caused about 140 ft of head decline in all three aquifer layers, which in turn, caused about 3 ft of permanent compaction of the aquifer system (and the same magnitude of land subsidence).
- From the late-1970s to 1990, heads in all three aquifer layers generally stabilized or increased, which caused the rates of compaction to virtually cease.
- From about 1989 to 1996, pumping from new deep wells in the Managed Area caused high magnitudes of head decline in the deep, confined aquifers of Layers 3 and 5, which caused about 2.4 ft of rapid compaction (and subsidence) within Layers 2, 3, 4 and 5. The subsidence was accompanied by ground fissuring, too.
- From 1996 to 2022, pumping from Layers 3 and 5 declined significantly, and by 2018, pumping from these deep, confined aquifers ceased. Pumping from Layer 1 also declined significantly during this period. The reduced pumping caused heads to recover significantly in all three aquifer layers. In particular, heads recovered by up to 400 ft in Layers 3 and 5, which in turn, caused compaction of the aquifer system to slow and then stop.

Figure 8b displays the vertical distribution of compaction and critical head by aquitard layer at the end of 1D model calibration (June 2022). The following observations and interpretations are made from Figure 8b:

- Critical heads are highest within the central portions of the thickest aquitards, which indicates that pore pressures within the thicker aquitards only partially equilibrated with the historical head declines in the adjacent aquifer layers, and hence, only partially compacted during the early 1990s when head declines were greatest.
- The highest critical heads within the aquitard layers are:
    - About 550 ft-amsl in Layers 1 and 2
    - About 450 ft-amsl in Layers 3, 4 and 5

- Additional compaction of the aquitard layers will occur if and when heads in the aquifers decline below the highest critical heads in the aquitards. However, heads in all aquifer layers in 2022 were higher than 580 ft-amsl (i.e., higher than the highest critical heads within the aquitard layers), which explains the recent observations of zero subsidence at this location.
- The Guidance Level that was established in the Subsidence Management Plan for heads in Layers 3 and 5 is about 400 ft-amsl, which is below the highest critical heads within some aquitard layers as shown in Figure 8b. If heads in Layers 3 and 5 were to decline to the Guidance Level, some permanent compaction of the aquitards may occur, but this compaction (and subsidence) would likely be of low magnitude and duration. The APX 1D model could be used to predict the magnitude and duration of compaction associated with heads maintained at the Guidance Level.

MODEL ERRORS AND LIMITATIONS

In general, a groundwater model is a simplified mathematical representation of a complex hydrogeologic system. Because of this, there are limits to the accuracy of the model and the use and interpretation of the model results. There are various sources of error and uncertainty. Model error commonly stems from the conceptual model, practical limitations of grid cell size and time discretization, parameter structure, insufficient calibration data, and the effects of processes not simulated by the model. These factors, along with error in observations, result in uncertainty in model results.

The potential errors and limitations associated with the 1D models and their calibration include:

- The 1D Models assume vertically one-dimensional deformation and groundwater flow within the modeled profile and therefore do not explicitly represent lateral variability in lithology, horizontal groundwater-flow gradients, or three-dimensional stress redistribution. Consequently, the calibrated aquitard properties should be interpreted as representative effective properties of the modeled location and may not be directly transferable to other locations within the Chino Basin.
- The 1D Models were based on the limited resolution, depth, and accuracy of the description of the aquifer-system sediments as documented on the driller's logs of Ontario Well 33, CCX, and APX boreholes.
- The resolution by depth interval of the lithologic descriptions are sometimes greater than five feet, which may not be a fine enough resolution to characterize any thinner interbedding of aquifer and aquitard layers that are an important control on aquifer-system deformation.

- The boreholes may not penetrate the full thickness of the semi-consolidated bedrock formations; there may be deforming sediments at depths below the borehole bottom that are responsible for some of the vertical ground motion estimated by InSAR.
- Most wells in the western Chino Basin have well screens that only penetrate the shallow aquifer-system or penetrate both the shallow and deep aquifer-systems. There are very few wells in the Northeast and Southeast Areas that are screened exclusively within the deep aquifer system and have records spanning the calibration period. As such, there is some uncertainty in the long-term time-series of heads for Layers 3 and 5 that were used as the boundary conditions for the 1D model calibration, which adds uncertainty to the model results. At the APX 1D model location, two of the extensometer wells and the Chino Hills 1B well are screened exclusively in the deep aquifer (layer 3, 5, or across both layers 3 and 5); however, water level measurements at these wells did not begin until well after the model calibration period began in 1930.
- Water-level data at wells is scarce in the Northeast Area, the Southeast Area, and the Managed Area prior to the 1930s. This 1D modeling effort assumed that the significant lowering of heads in all three areas began after 1930, which may not be an accurate assumption. If head declines began before 1930, then this could impact the calibration of the 1D models and add uncertainty to the model results.
- The 1D models used a combination of benchmark, extensometer, and InSAR-derived estimates of vertical ground motion as calibration targets for aquifer-system compaction, all of which have limitations:
    - The limitations of using benchmark data as calibration targets are: (1) benchmark surveys are typically collected infrequently, resulting in relatively low temporal resolution compared to groundwater-level measurements and extensometer data; (2) benchmark measurements represent cumulative land-surface elevation change between surveys and therefore provide limited information regarding the timing of subsidence within the survey interval; (3) benchmark elevations may be affected by surveying error, monument instability, or local near-surface processes unrelated to aquifer-system compaction; and (4) benchmark measurements represent deformation at a single location and may not be representative of conditions across the broader area surrounding the benchmark.
    - The limitation of using extensometer data as calibration targets are: (1) extensometers only measure compaction occurring within the instrumented interval and may not capture deformation occurring above or below that interval; (2) instrument drift, maintenance issues, and changes in measurement procedures may introduce uncertainty into long-term records; (3) extensometer records are often shorter than the simulation period and

therefore do not provide calibration targets for the full duration of the model; and (4) compaction measured by an extensometer may not be directly representative of total land-surface subsidence because deformation may occur outside the monitored depth interval.

- The limitations of using InSAR-derived estimates as calibration targets are: (1) the InSAR record begins in 1992, which limits the length of the calibration period; (2) there are multiple data gaps in the InSAR record because of satellite malfunctions and satellite replacement; and (3) InSAR produces an aggregate estimate of aquifer-system deformation and therefore provides no depth-specific calibration targets. Due to the lack of depth-specific calibration there is greater uncertainty in the depth-specific estimates for the aquifer and aquitard properties, and hence, the model results.

REFERENCES

Hoffmann, J., Leake, S.A.; Galloway, D.L.; Wilson, M.A. (2003). *MODFLOW-2000 Ground-water model--user guide to the Subsidence and Aquifer-System Compaction (SUB) Package.* Open File Report 03-233. - Tucson, AZ : U.S. Geological Survey, 2003.

Leake S. A. and Prudic D. E. (1991) *Documentation of a computer program to simulate aquifer-system compaction using the modular finite-difference ground-water flow model.* Techniques of Water-Resources Investigations 06-A2. - [s.l.] : U. S. Geological Survey, 1991.

Leake S. A. and Lilly M. R. (1997) *Documentation of a Computer Program (FHB1) for Assignment of Transient Specified-Flow and Specified-Head Boundaries in Applications of the Modular Finite-Difference Ground-Water Flow Model (MODFLOW).* Open-File Report 97-571. - Tucson, Arizona : U. S. Geological Survey, 1997.

Meade, R.H., 1964, *Removal of water and rearrangement of particles during the compaction of clayey sediments—review*: U.S. Geological Survey Professional Paper 497-B, 23 p.

Niswonger, R. G., Panday, S., & Ibaraki, M. (2011). *MODFLOW-NWT, A Newton formulation for MODFLOW-2005: U.S. Geological Survey Techniques and Methods 6-A37, 44 p.* Reston, Virginia: U.S. Geological Survey.

Riley, F.S. (1969). *Analysis of borehole extensometer data from central California*: International Association of Scientific Hydrology Publication 89, p. 423–431.

———(1998). *Mechanics of aquifer systems—The scientific legacy of Dr. Joseph F. Poland, in Borchers, J.W., ed., Land subsidence case studies and current research*: Proceedings of the Dr. Joseph F. Poland Symposium on Land Subsidence, Association of Engineering Geologists Special Publication no. 8, p. 13–27.

Wildermuth Environmental Inc. (2017). *Technical Memorandum. Task 3 and Task 4 of the Work Plan to Develop a Subsidence Management Plan for the Northwest MZ-1 Area: Development and Evaluation of Baseline and Initial Subsidence-Management Alternatives.*

Wildermuth Environmental Inc. (2020). *2020 Safe Yield Recalculation Final Report. Prepared for Chino Basin Watermaster.*

Appendix A

Driller's Logs of Ontario Well 33, CCX, and APX Extensometers

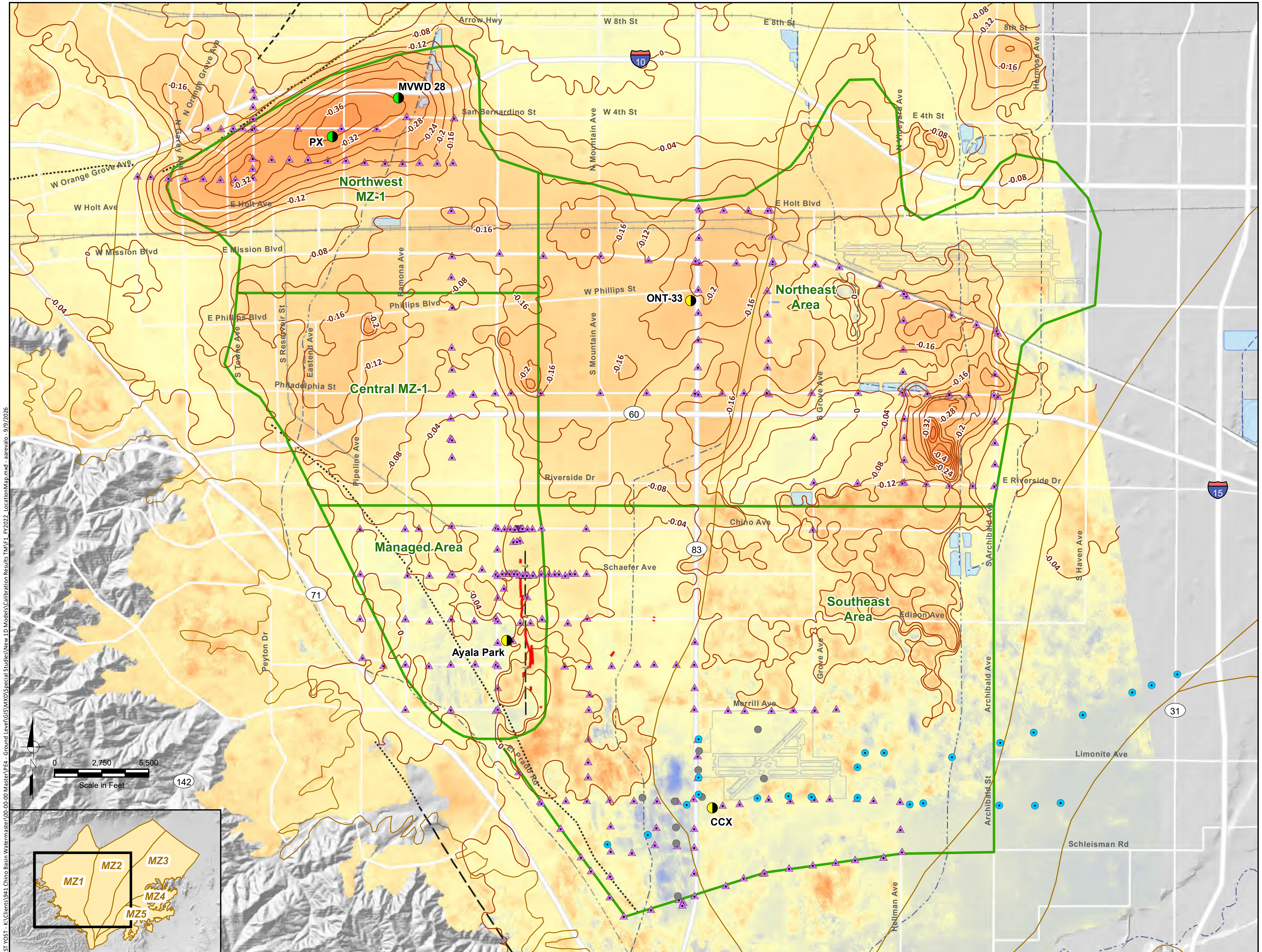

Areas of Subsidence Concern

Chino Desalter Authority Well

SB County Proposed Extraction Well

Ground-Level Survey Benchmark

Ground Fissures

Approximate Location of the Riley Barrier

1D Compaction Model Locations

Existing

New

Relative Change in Land Surface Altitude as Estimated by InSAR (March 2011 to March 2022)

+ 0.55 ft

0 ft

-0.20

-0.55 ft

InSAR absent or incoherent

WEST YOST

Chino Basin Watermaster
Construction/Calibration of Additional 1D Compation Models

Figure 1
Locations of One-Dimensional Compaction Models

WEST YOST - K:\Clients\941 Chino Basin Watermaster\00-00-00 Master\PE4 - Ground Level\GIS\MXD\Special Studies\New 1D Models\Calibration Results TM\F1_FY2022_LocationMap.mxd - aarevalo - 9/9/2026

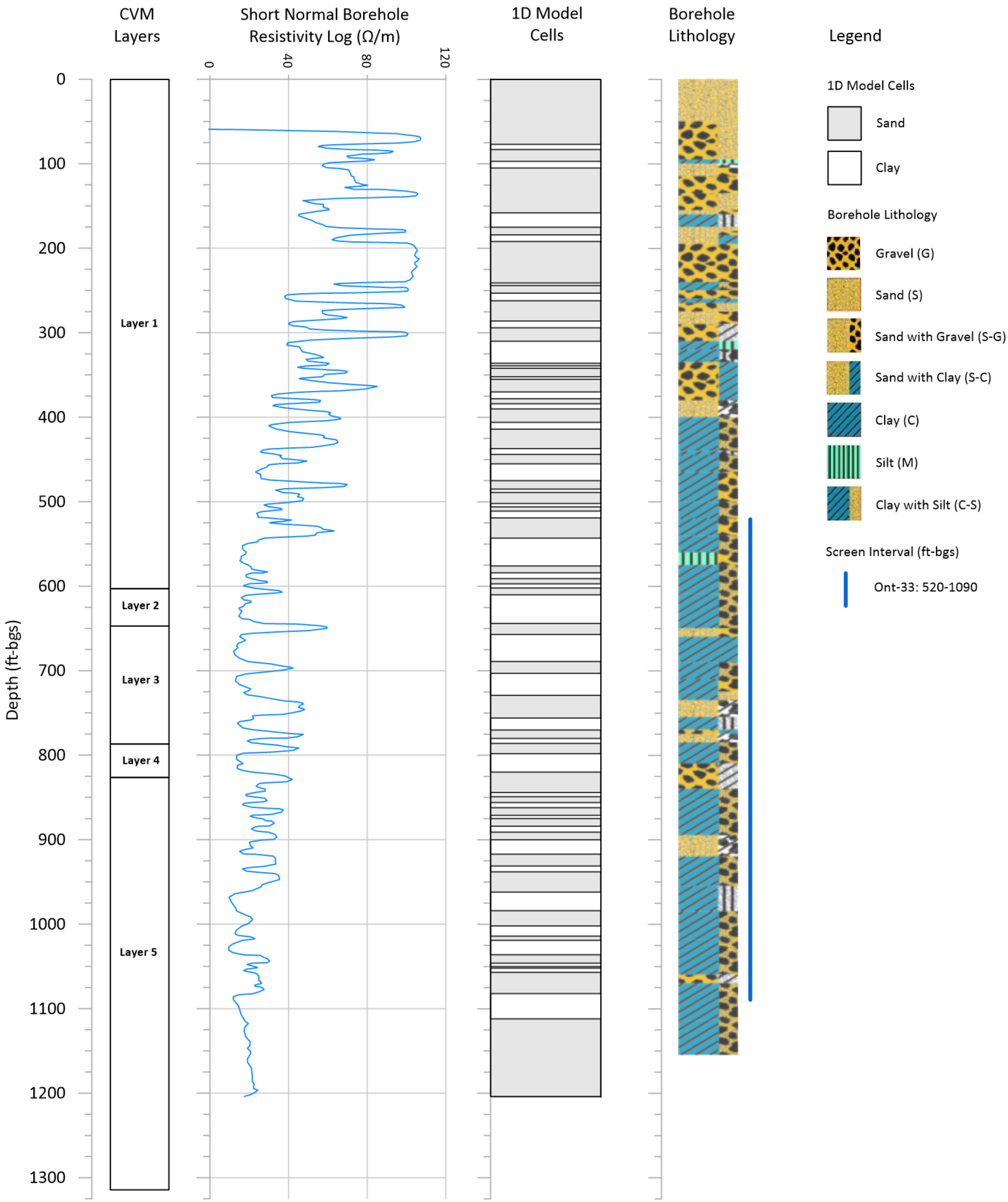

File: Figure3a_Ont33_Logs.grf; Date: 9/11/2026; Author: CK

Prepared by:

WEST YOST
Water. Engineered.

Prepared for:

Chino Basin Watermaster
Construction/Calibration of
Additional 1D Compaction Models

Structure of 1D Model
ONT-33

Figure 2a

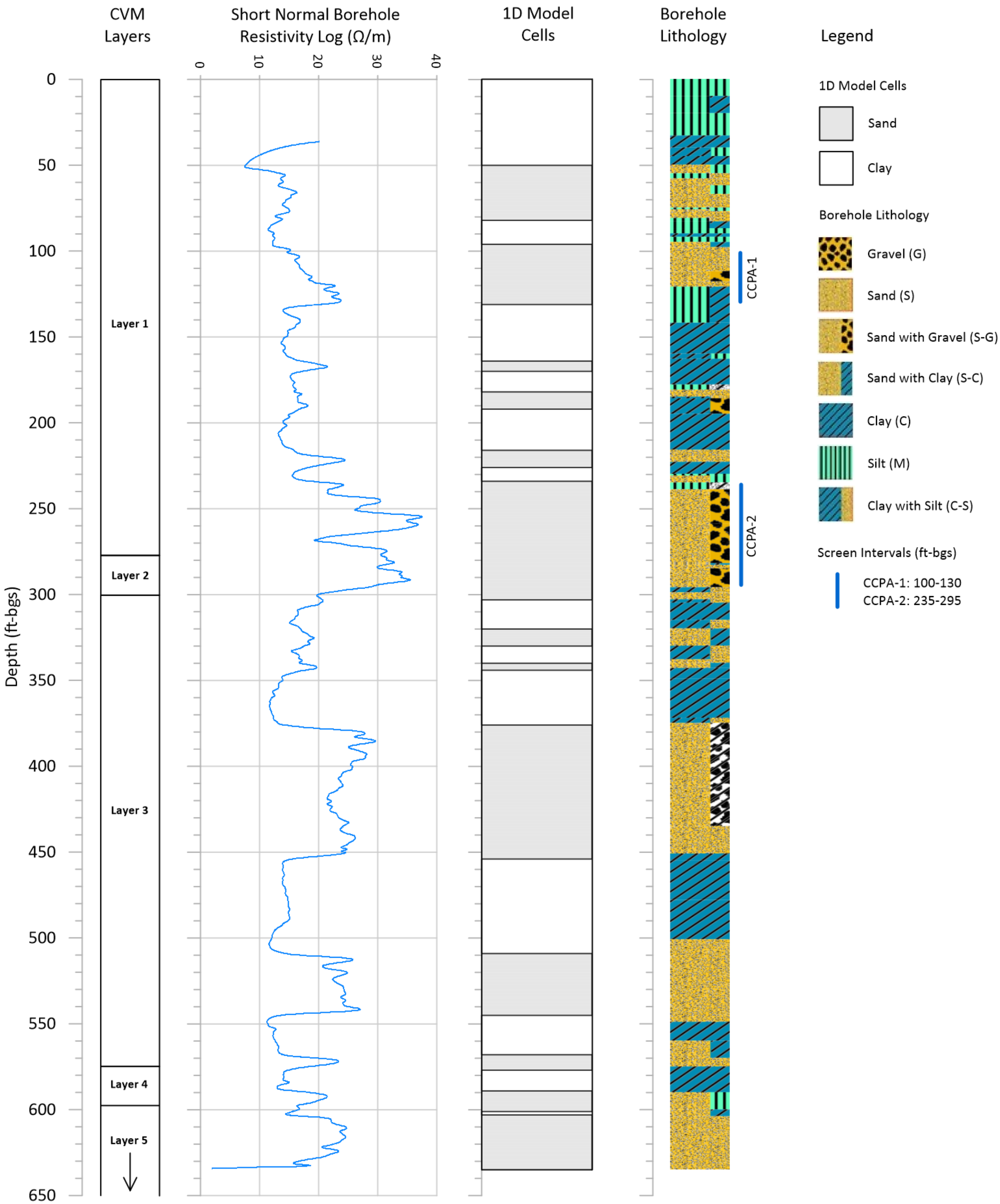

File: Figure3b_CCX_Logs.grf; Date: 9/11/2026; Author: CK

Prepared by:

WEST YOST
Water. Engineered.

Prepared for:

Chino Basin Watermaster
Construction/Calibration of
Additional 1D Compaction Models

Structure of 1D Model
CCX

Figure 2b

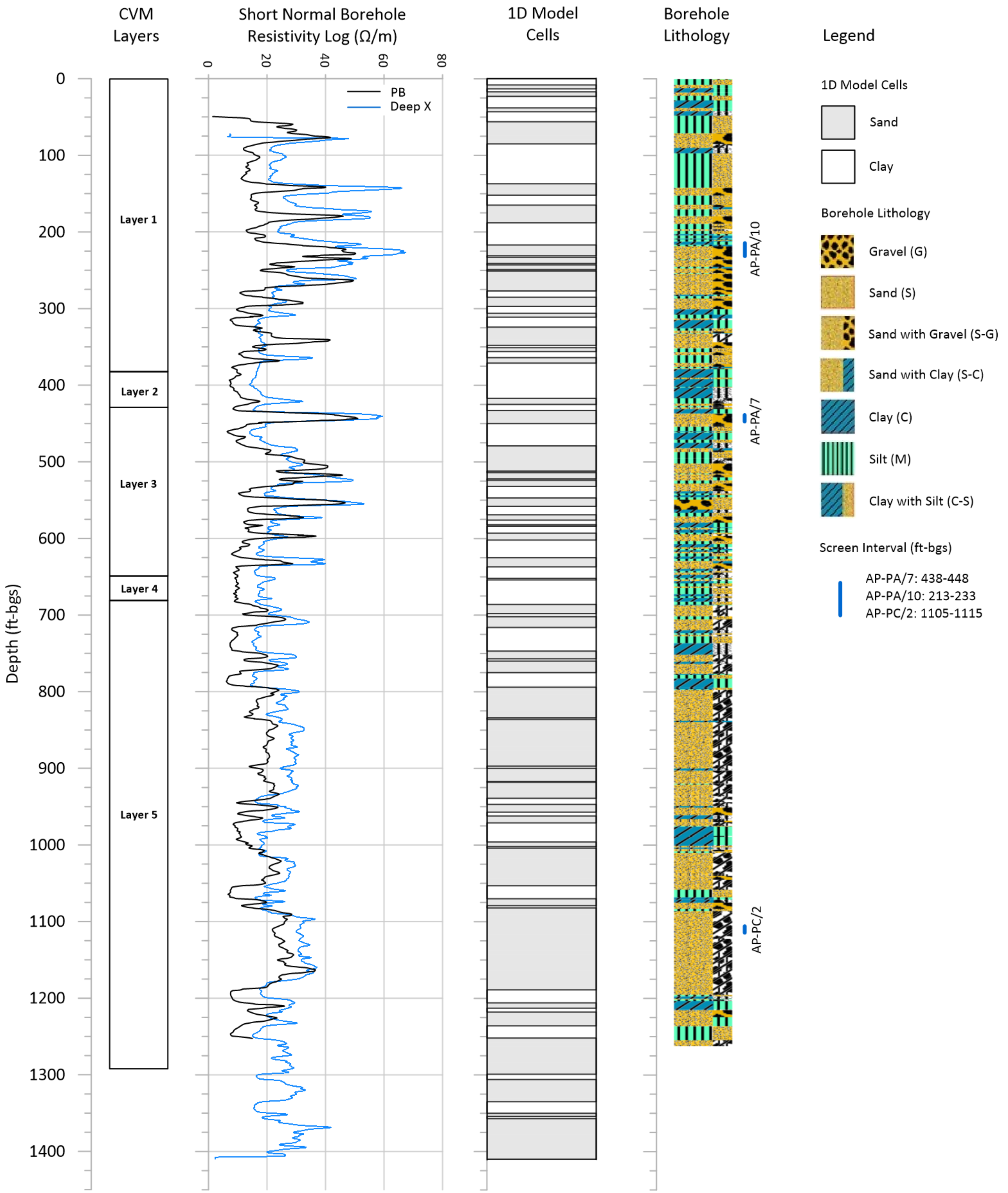

File: Figure3c_Ayala_Logs.grf; Date: 9/11/2026; Author: CK

Prepared by:

WEST YOST
Water. Engineered.

Prepared for:

Chino Basin Watermaster
Construction/Calibration of
Additional 1D Compaction Models

Structure of 1D Model
APX

Figure 2c

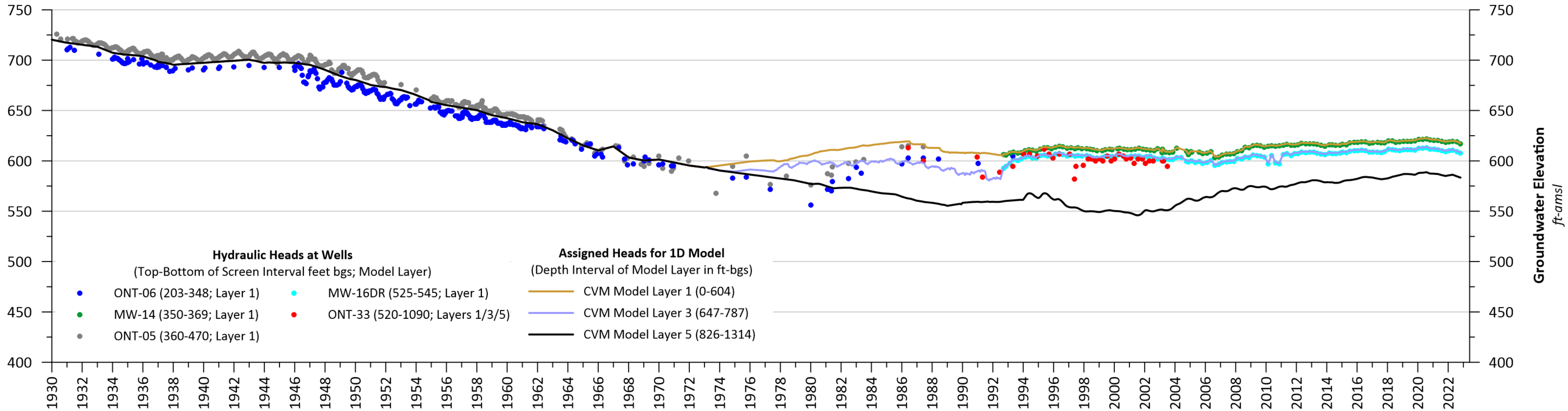

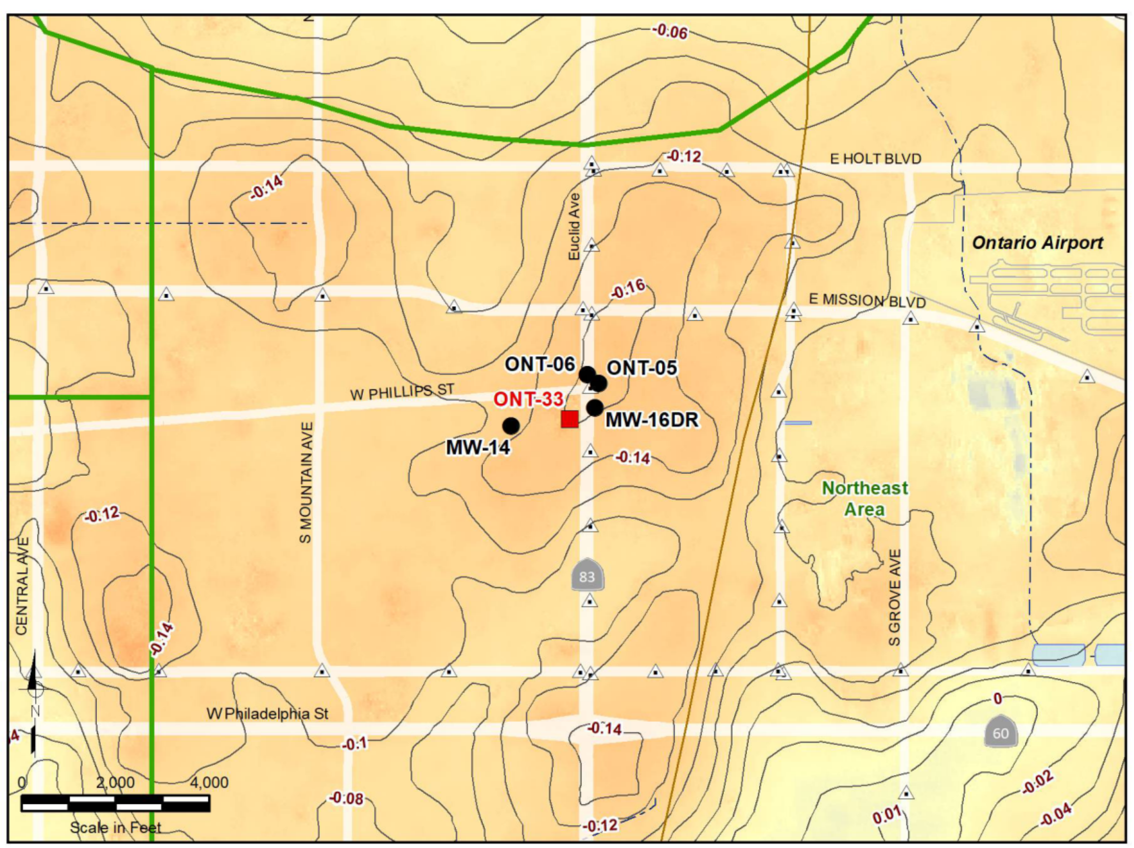

InSAR from March 2011 to March 2022 (see Figure 2)

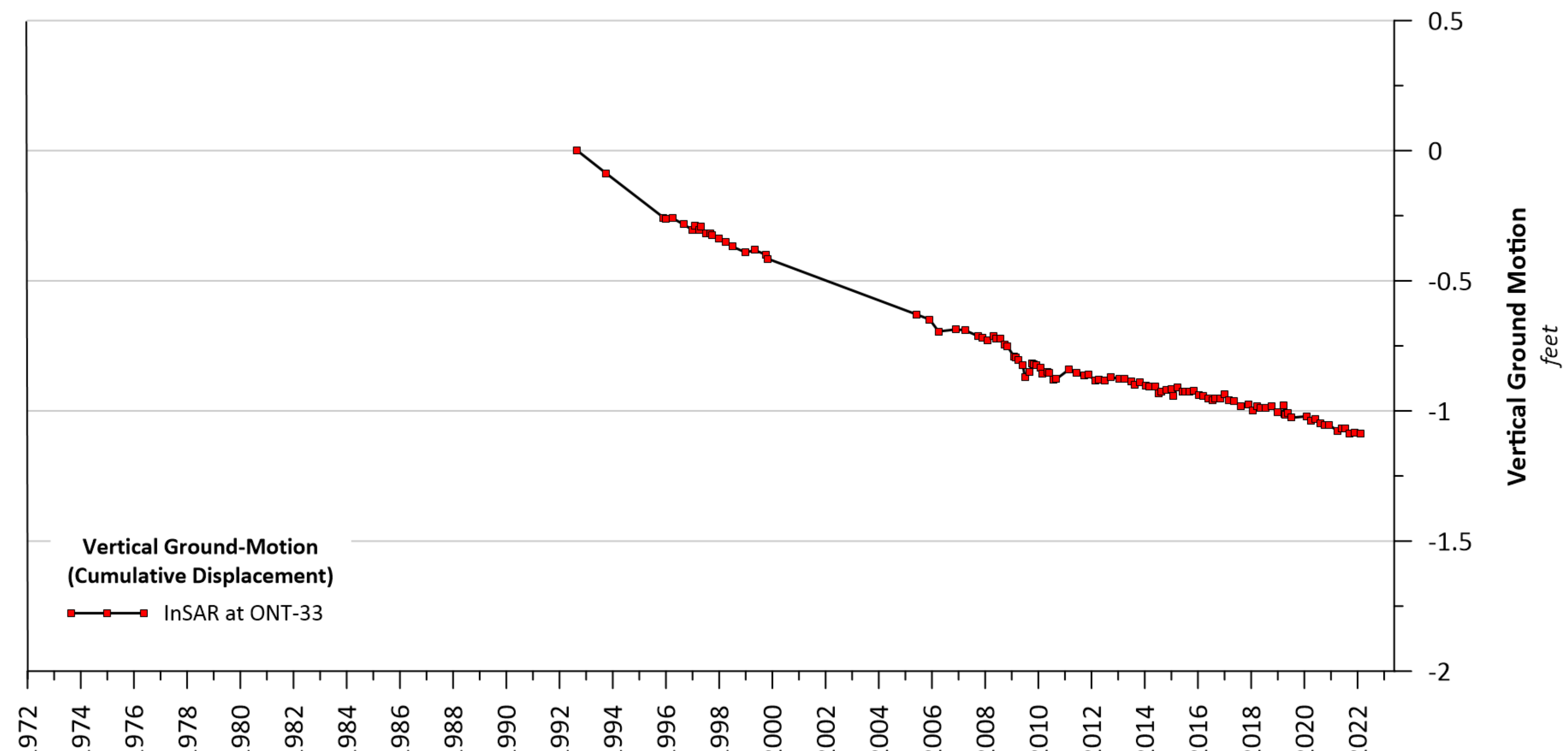

Prepared by:

WEST YOST Water. Engineered.

File: Figure4_Ont33.grf
Date: 9/11/2026
Author: CK

Prepared for:
Chino Basin Watermaster
Construction/Calibration of Additional
1D Compaction Models

Historical Data for Calibration of the 1D Model
ONT-33

Figure 3a

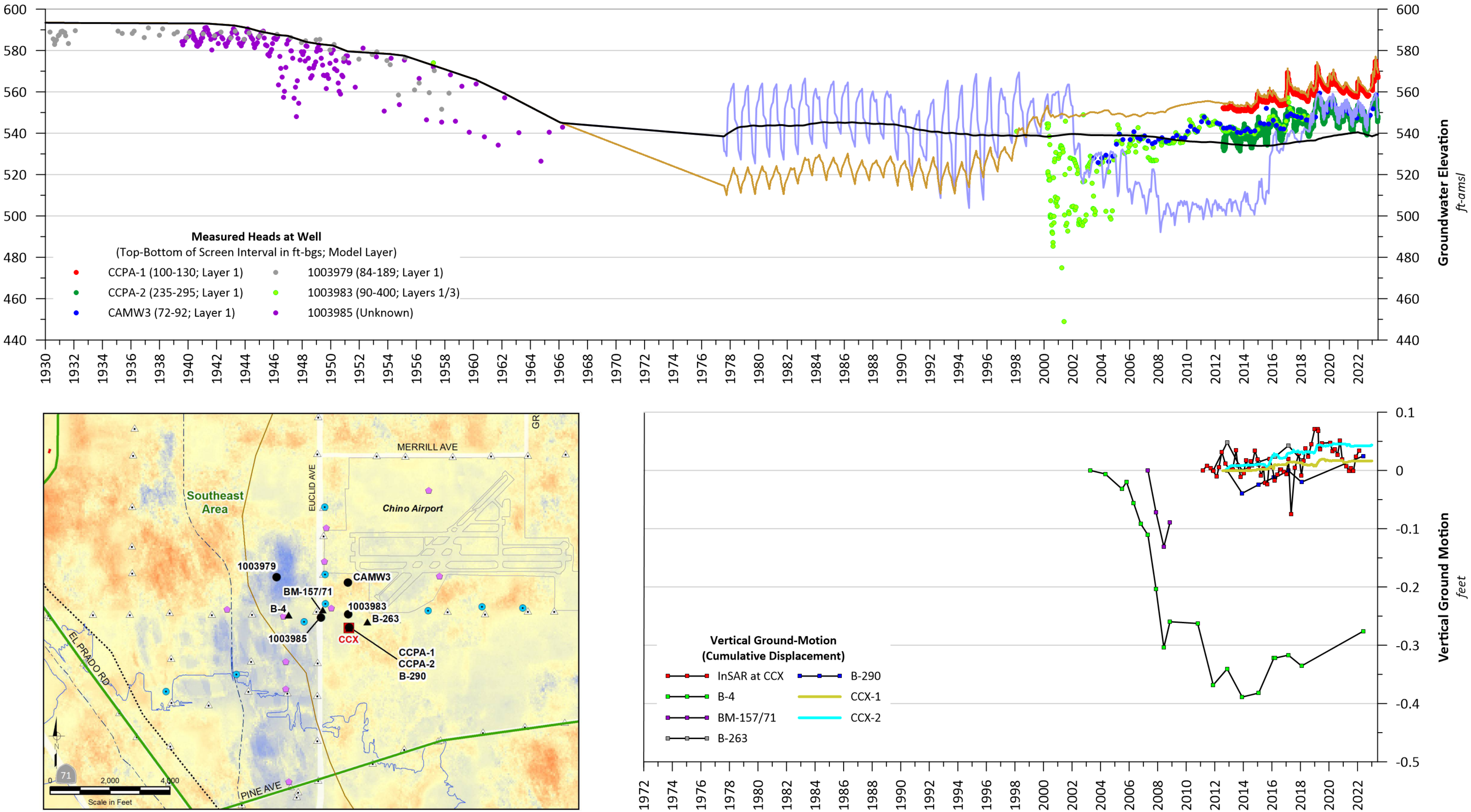

InSAR from March 2011 to March 2022 (see Figure 2)

Prepared by:

WEST YOST
Water. Engineered.

File: Figure6_CCX.grf
Date: 9/11/2026
Author: CK

Prepared for:
Chino Basin Watermaster
Construction/Calibration of Additional
1D Compaction Models

Historical Data for Calibration of the 1D Model
CCX

Figure 3b

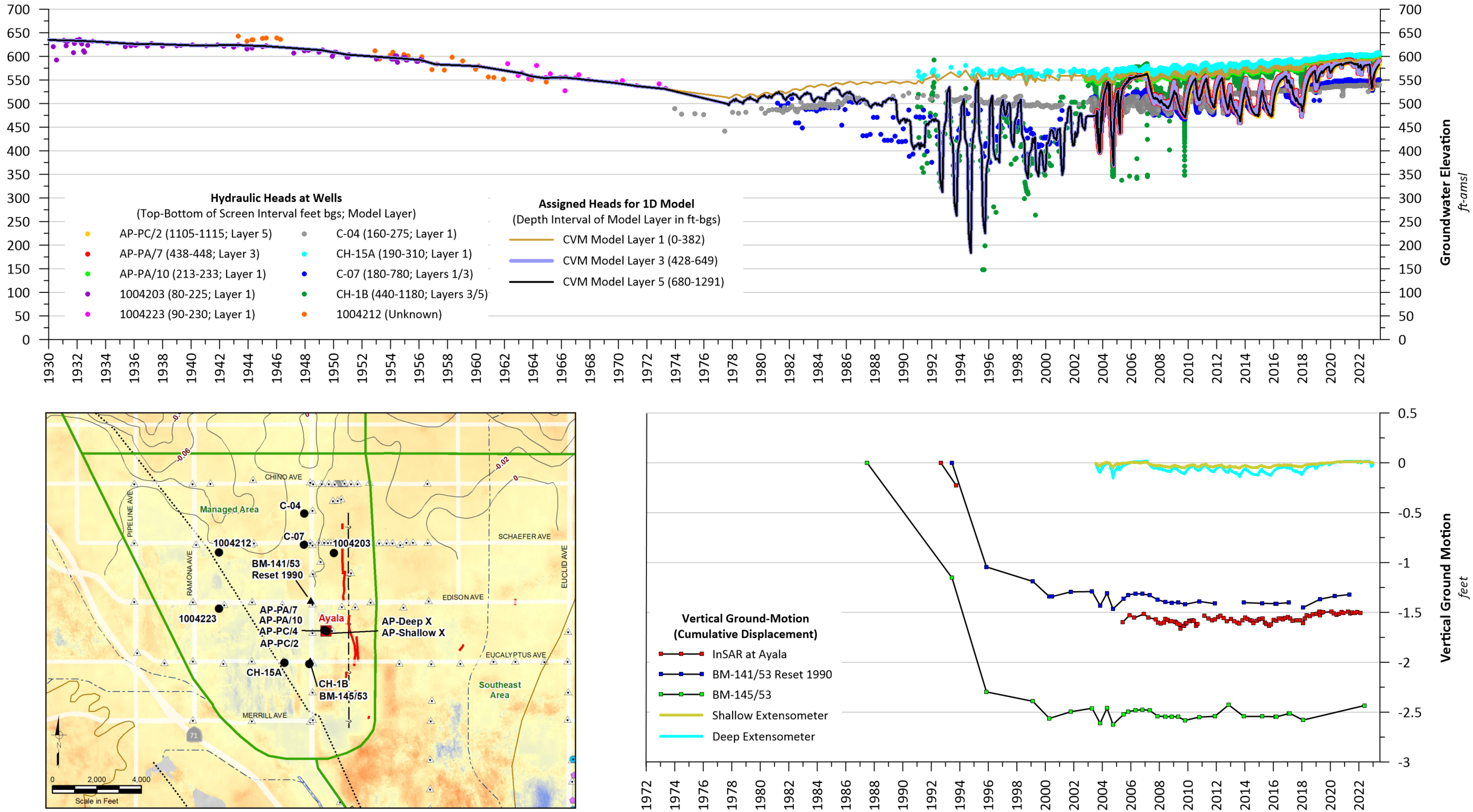

InSAR from March 2011 to March 2022 (see Figure 2)

Prepared by:

WEST YOST
Water. Engineered.

File: Figure8_Ayala.grf
Date: 9/11/2026
Author: CK

Prepared for:
Chino Basin Watermaster
Construction/Calibration of Additional
1D Compaction Models

Historical Data for Calibration of the 1D Model
APX
Figure 3c

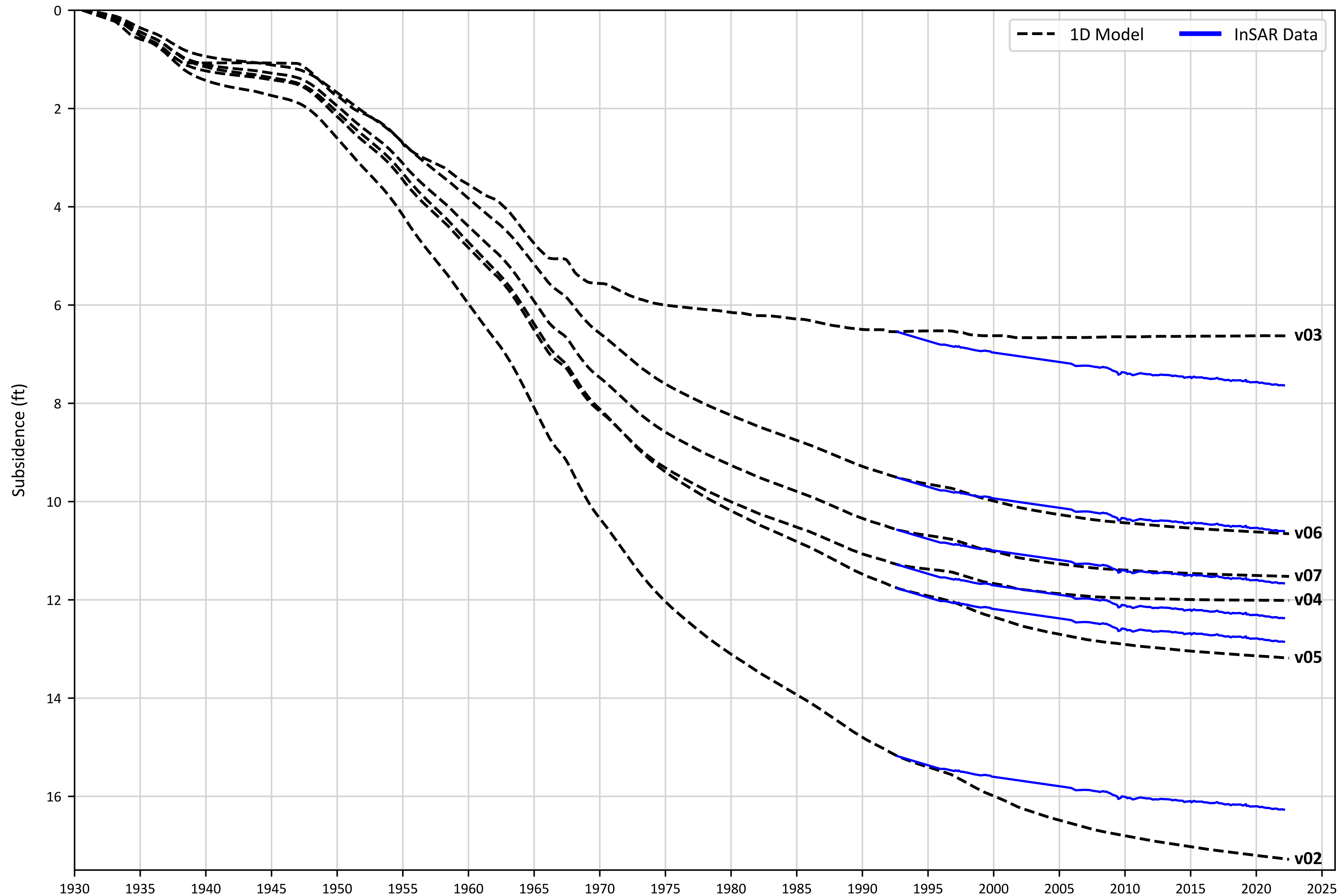

Prepared by:

WEST YOST

Prepared for:

Chino Basin Watermaster

Construction/Calibration of Additional
1D Compaction Models

Time Series of the Simulated and Observed Subsidence Values for Select Model Versions
ONT-33

Figure 4a

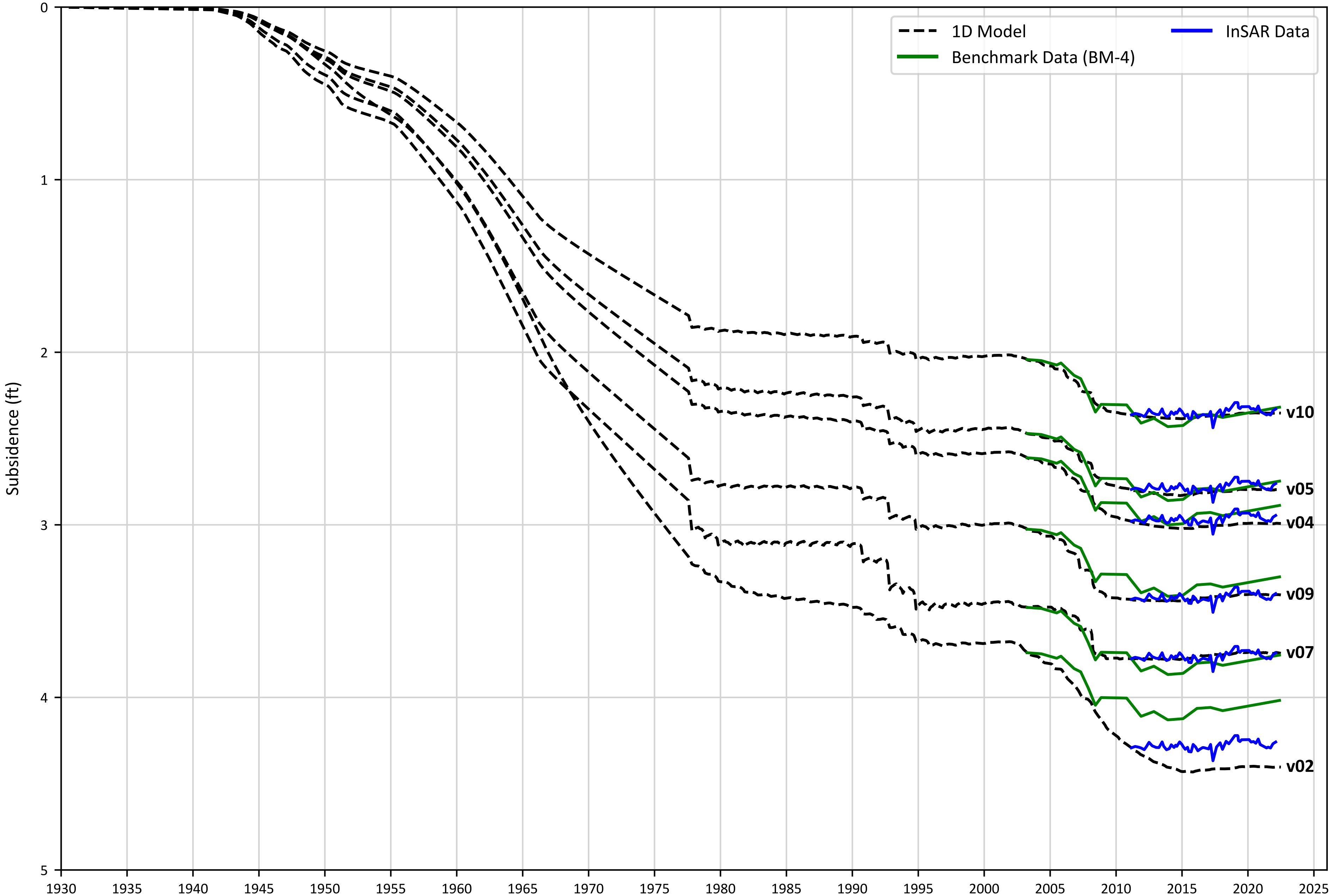

Prepared by:

WEST YOST

Prepared for:

Chino Basin Watermaster

Construction/Calibration of Additional
1D Compaction Models

Time Series of the Simulated and Observed Subsidence Values for Select Model Versions
CCX

Figure 4b

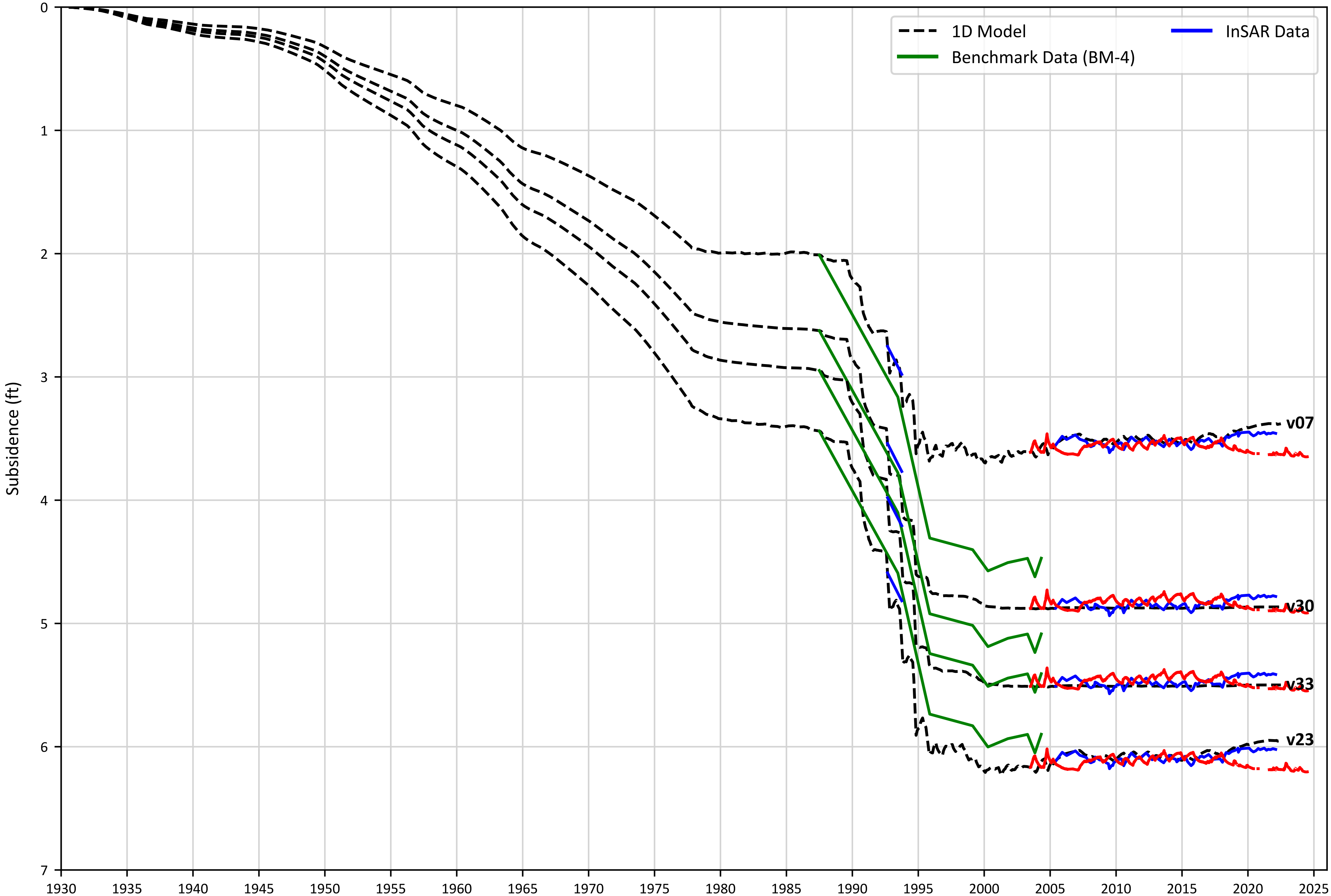

Prepared by:

WEST YOST

Prepared for:

Chino Basin Watermaster

Construction/Calibration of Additional 1D Compaction Models

Time Series of the Simulated and Observed Subsidence Values for Select Model Versions APX

Figure 4c

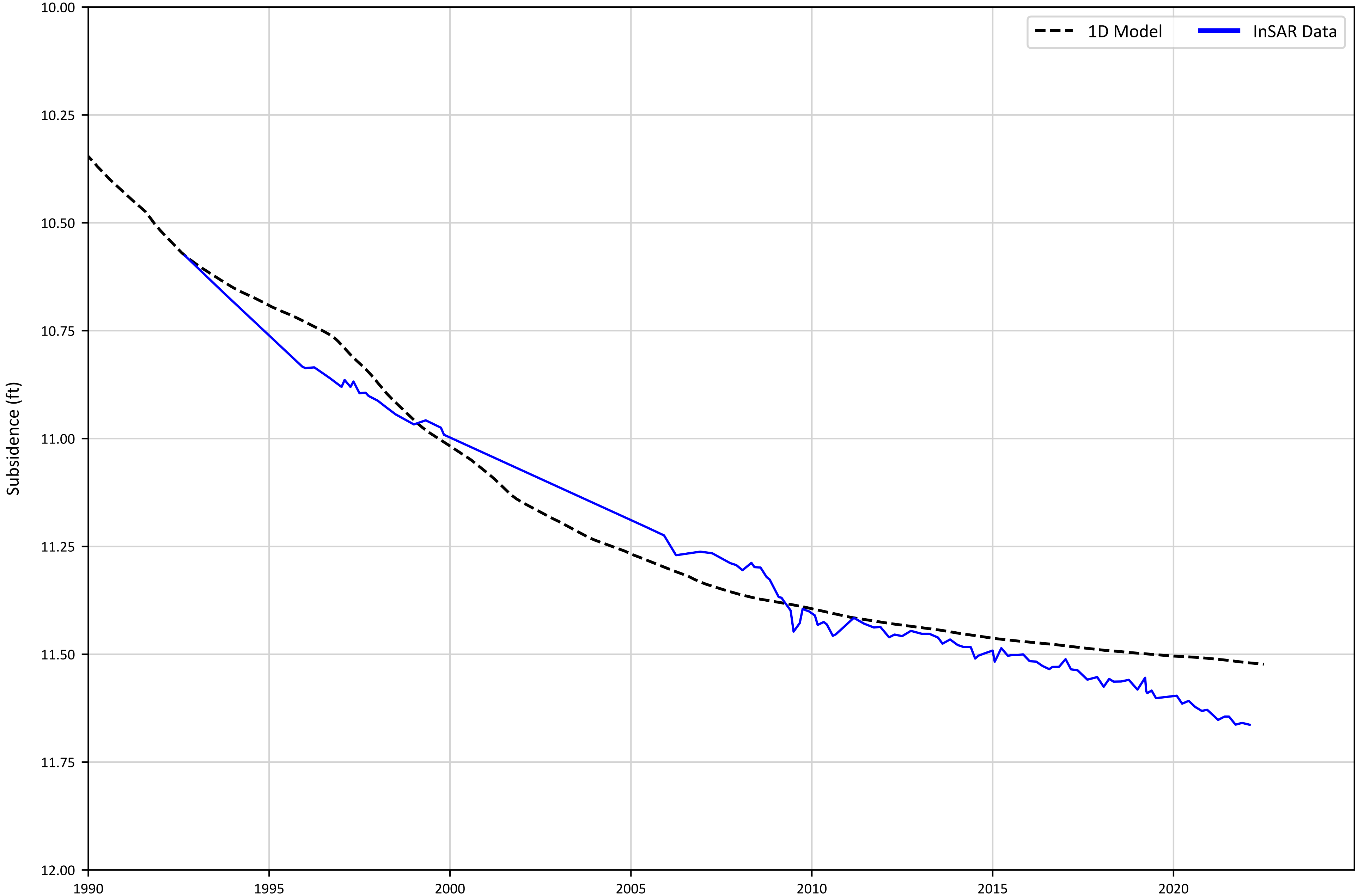

Prepared by:

WEST YOST

Prepared for:

Chino Basin Watermaster

Construction/Calibration of Additional
1D Compaction Models

Time Series of the Simulated and Observed Subsidence Values from 1990 to 2024
ONT-33

Figure 5a

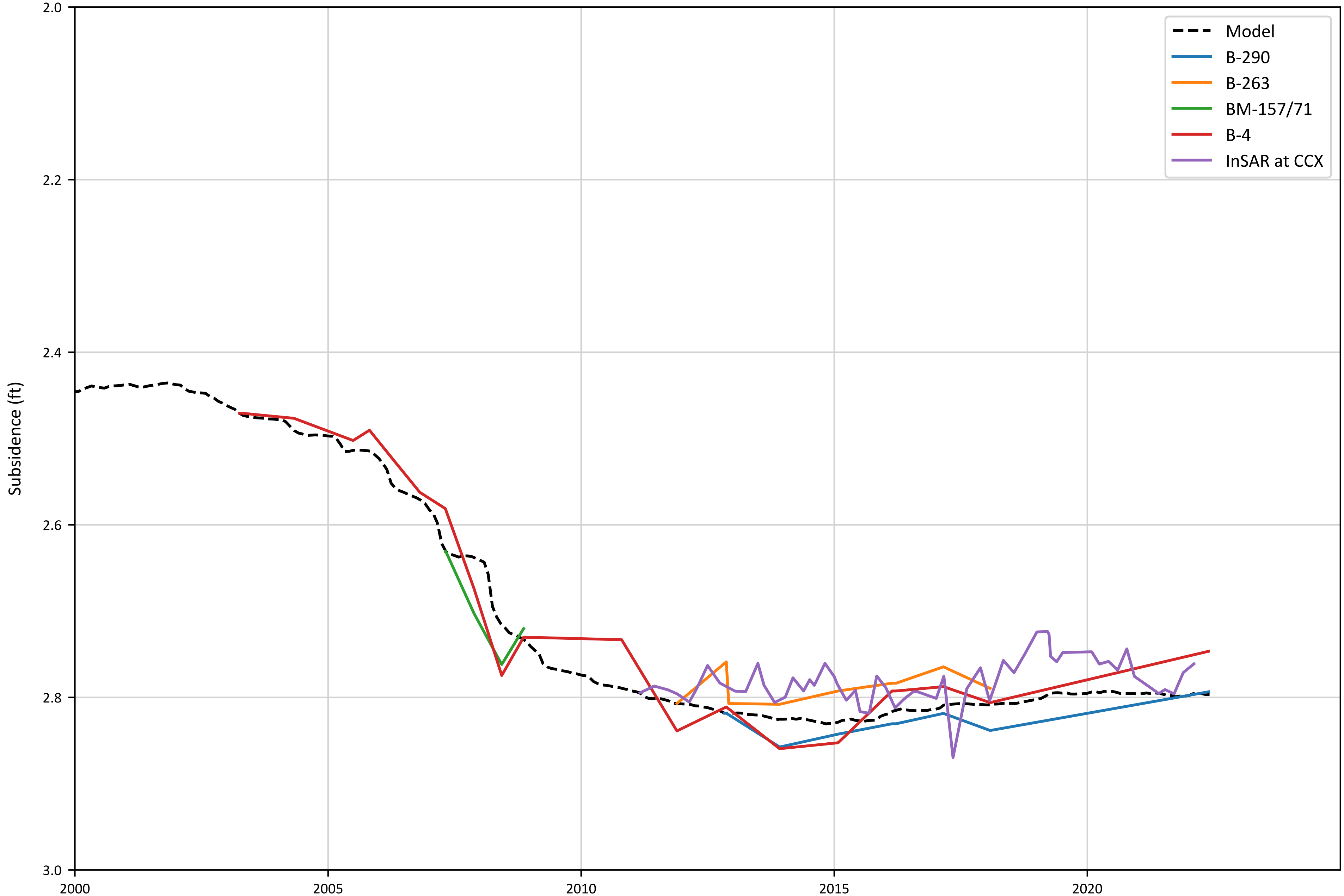

Prepared by:

WEST YOST

Prepared for:

Chino Basin Watermaster

Construction/Calibration of Additional
1D Compaction Models

Time Series of the Simulated and Observed Subsidence Values from 1985 to 2024

CCX - V05

Figure 5b

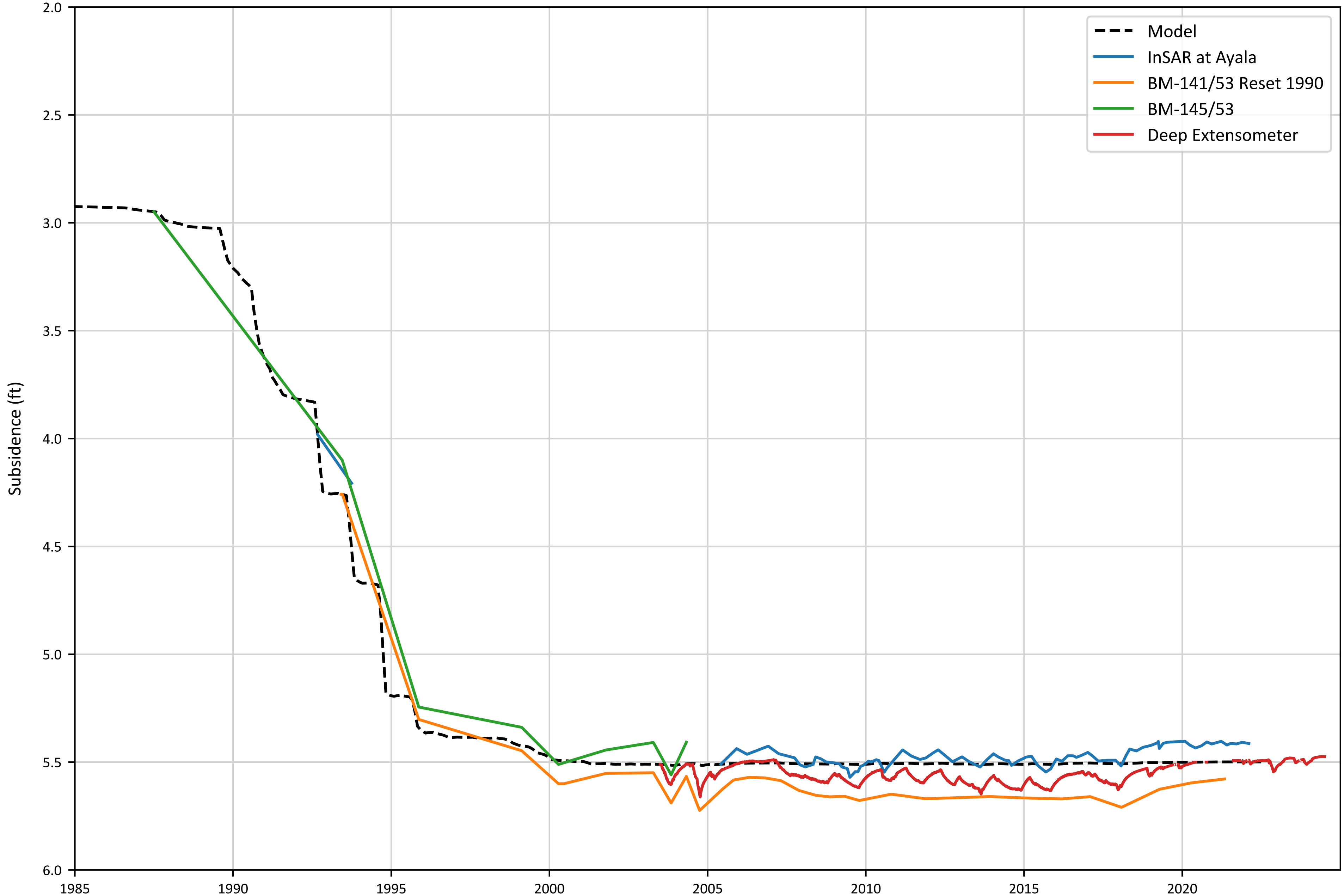

Prepared by:

WEST YOST

Prepared for:

Chino Basin Watermaster

Construction/Calibration of Additional
1D Compaction Models

Time Series of the Simulated and Observed Subsidence Values from 1985 to 2024

APX - V33

Figure 5c

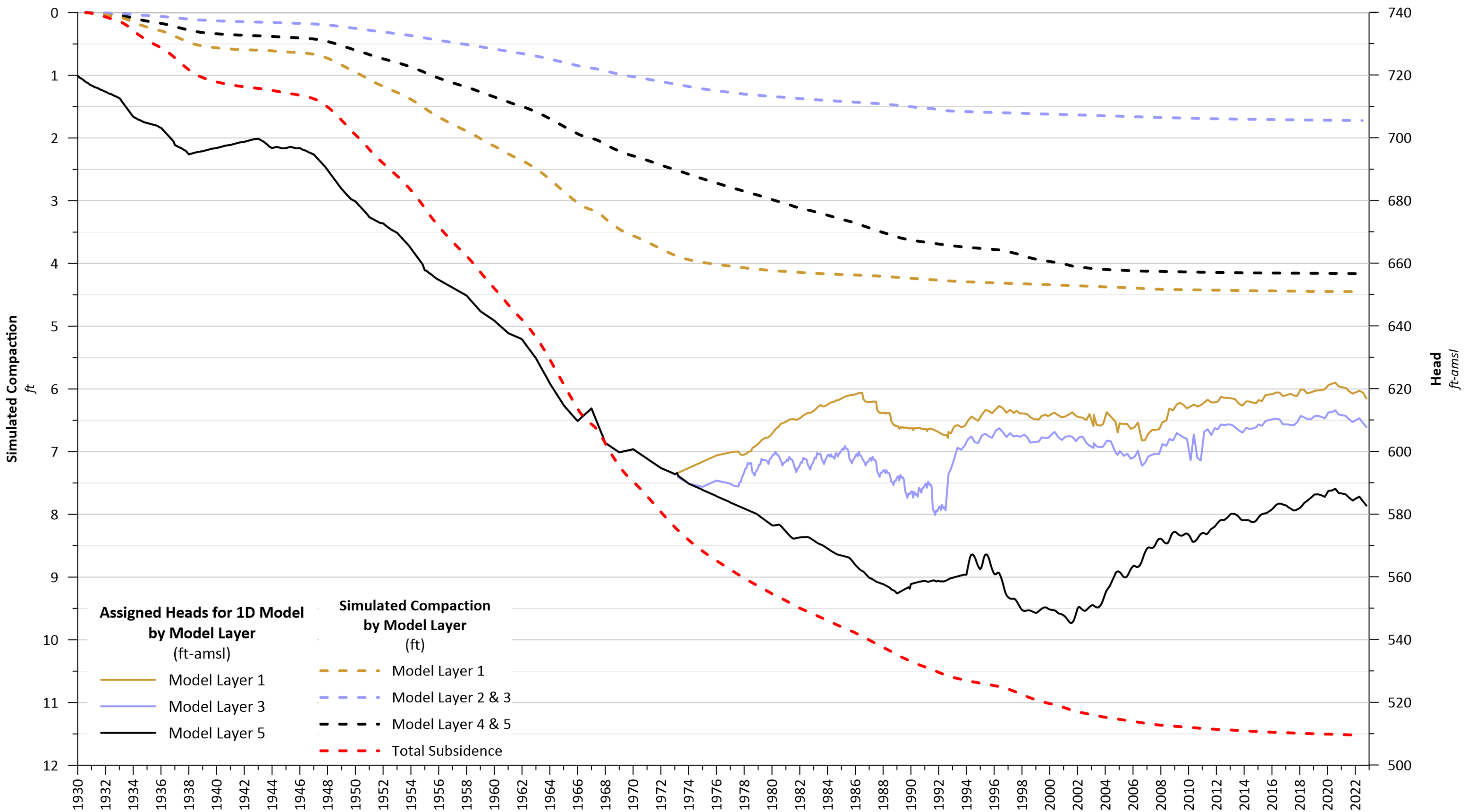

Prepared by:

WEST YOST
Water. Engineered.

File: Figure9a_Ont33.grf
Date: 9/16/2026
Author: CK

Prepared for:
Chino Basin Watermaster
Construction/Calibration of Additional 1D Compaction Models

Simulated Head and Compaction
ONT-33 - v07

Figure 6a

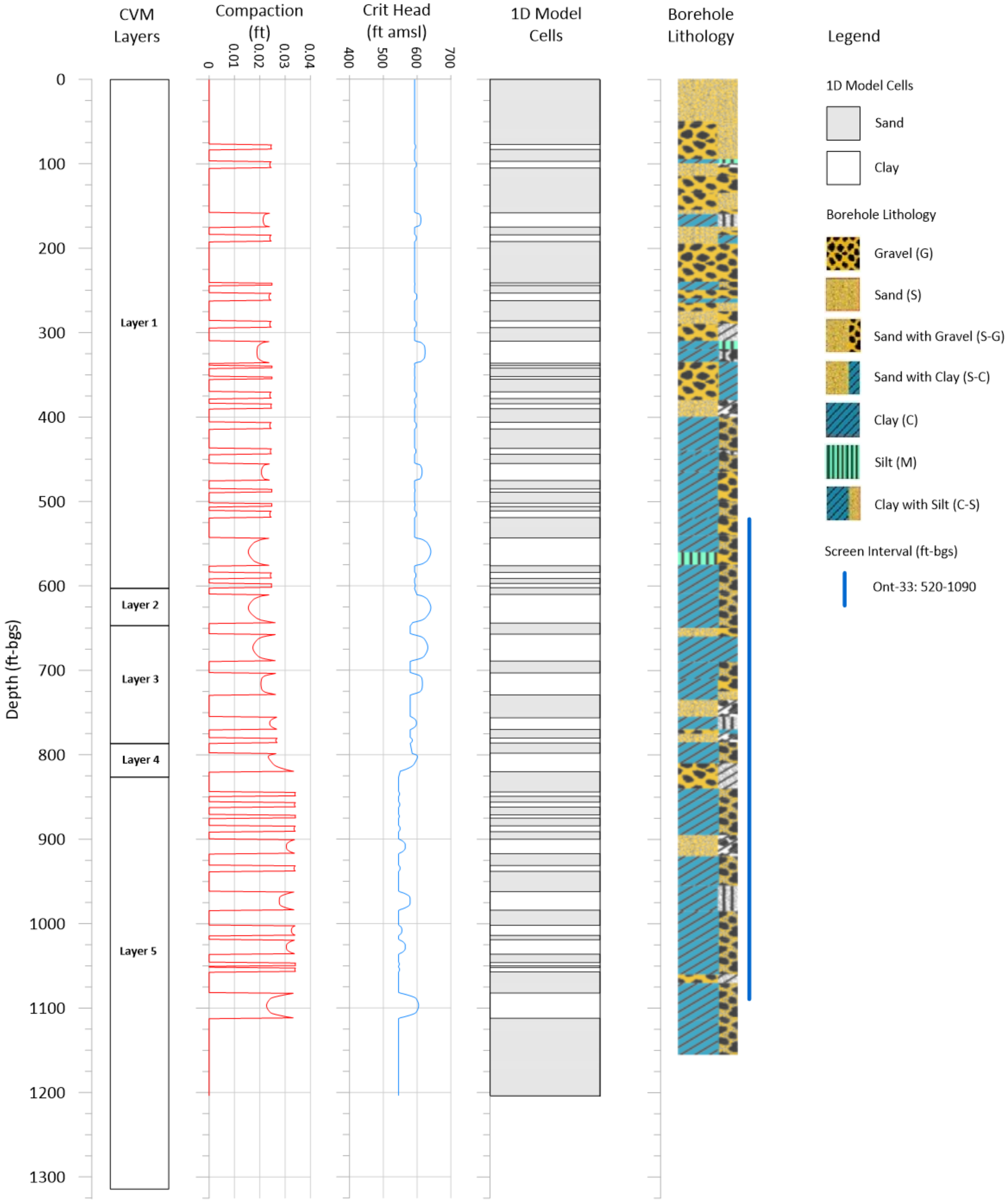

File: Figure8a_Ont33_Log_Compaction_CritHead.grf; Date: 9/11/2026; Author: CK

Prepared by:

WEST YOST
Water. Engineered.

Prepared for:

Chino Basin Watermaster
Construction/Calibration of
Additional 1D Compaction Models

Simulated Compaction and Critical Head on June 2022
ONT-33 - v07

Figure 6b

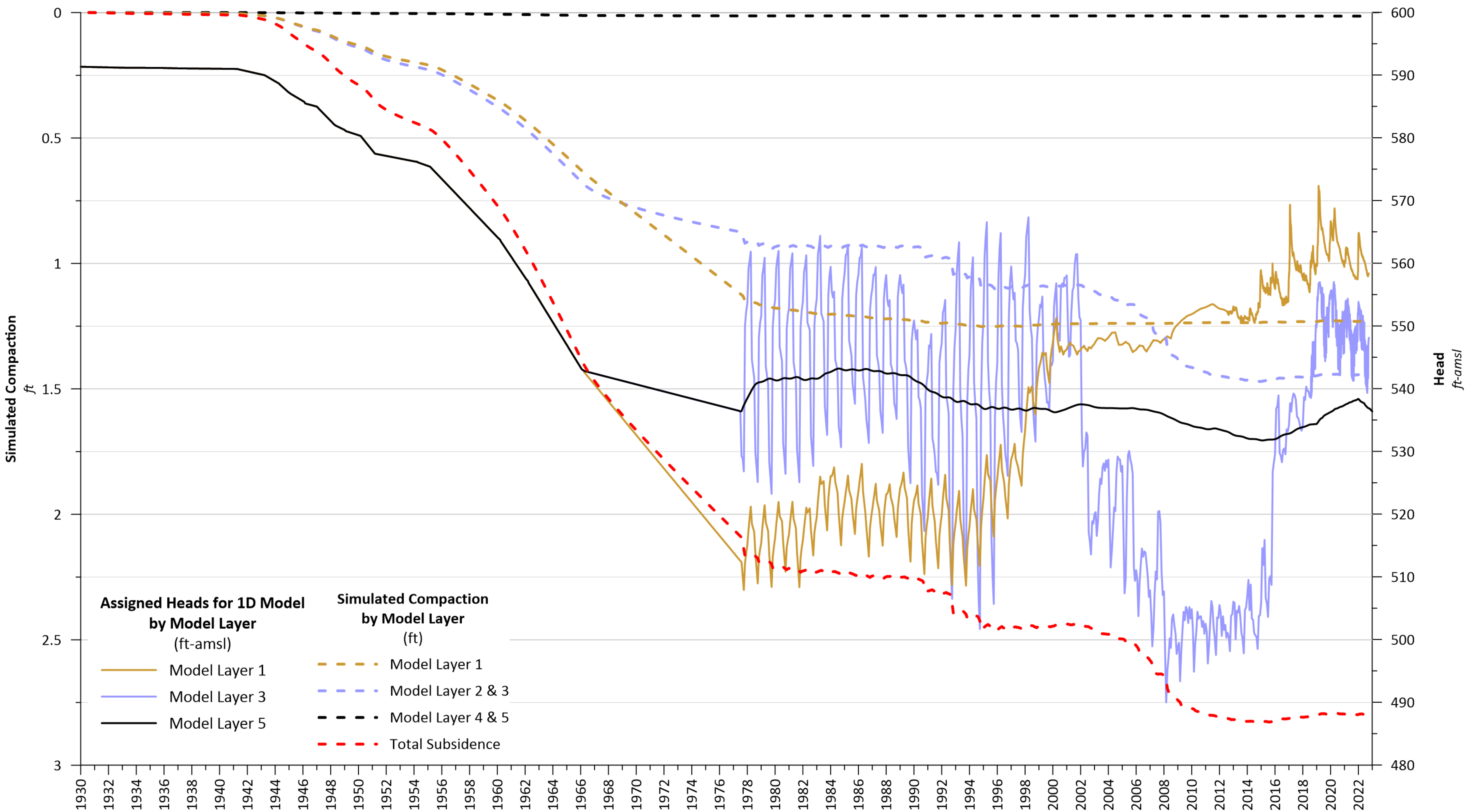

Prepared by:

WEST YOST
Water. Engineered.

File: Figure8b_CCX.grf
Date: 9/16/2026
Author: CK

Prepared for:
Chino Basin Watermaster
Construction/Calibration of Additional
1D Compaction Models

Simulated Head and Compaction
CCX - v05

Figure 7a

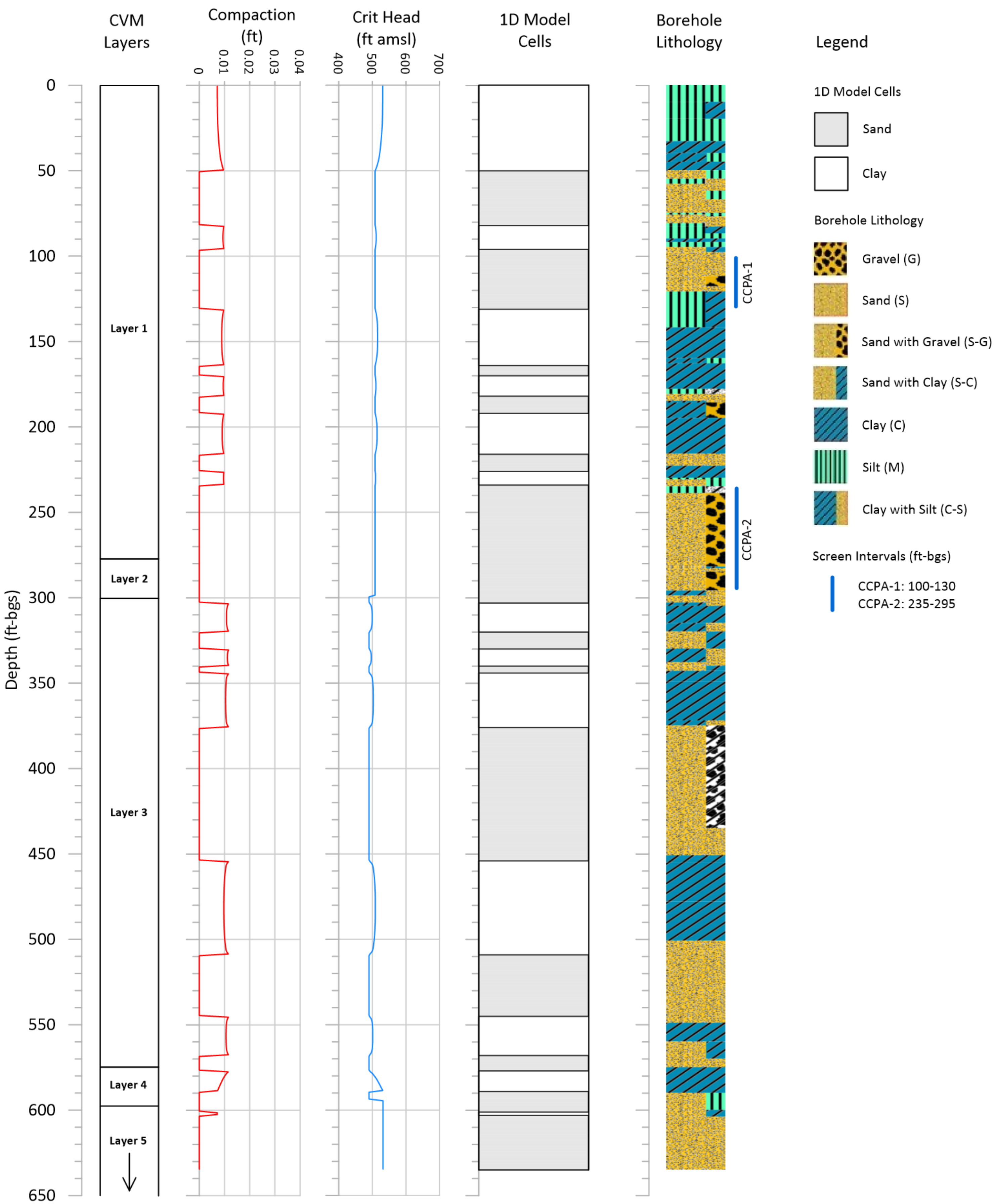

File: Figure8b_CCX_Log_Compaction_CritHead.grf; Date: 9/11/2026; Author: CK

Prepared by:

WEST YOST
Water. Engineered.

Prepared for:

Chino Basin Watermaster
Construction/Calibration of
Additional 1D Compaction Models

Simulated Compaction and Critical Head on June 2022
CCX - v05

Figure 7b

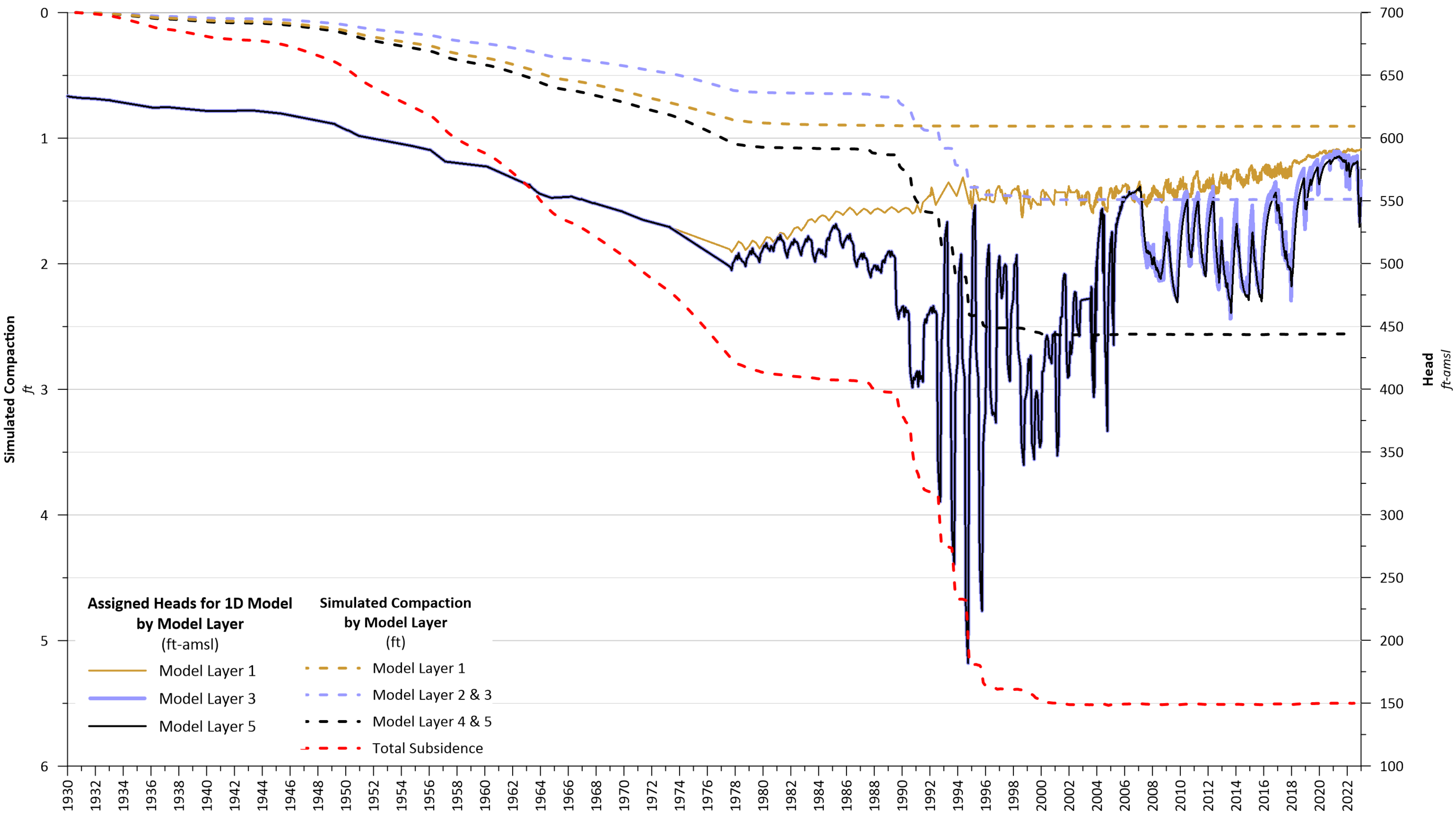

Prepared by:

WEST YOST
Water. Engineered.

File: Figure8c_APX.grf
Date: 9/16/2026
Author: CK

Prepared for:
Chino Basin Watermaster
Construction/Calibration of Additional 1D Compaction Models

Simulated Head and Compaction
APX - v33

Figure 8a

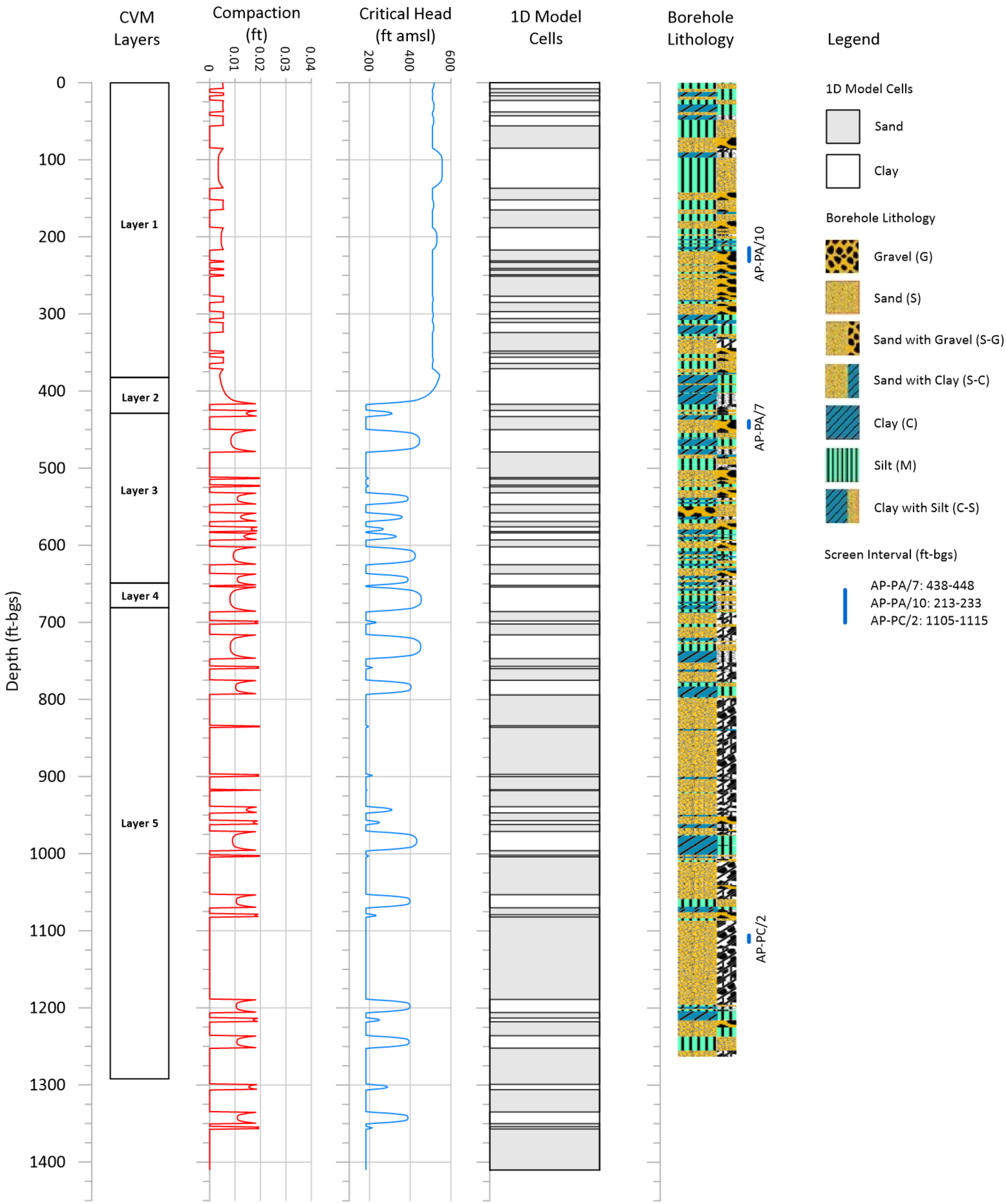

File: Figure8c_APX_Log_Compaction_CritHead.grf; Date: 9/11/2026; Author: CK

Prepared by:

WEST YOST
Water. Engineered.

Prepared for:

Chino Basin Watermaster
Construction/Calibration of
Additional 1D Compaction Models

Simulated Compaction and Critical Head on June 2022
APX - v33

Figure 8b

Table 3a. Aquitard Properties for Clay Cells by Calibration Iteration -- ONT-33				
Iteration	VK [ft/day]	Ss [1/ft]	Sfv [-]	Sfe [-]
v00	2.50E-05	1.14E-05	1.65E-04	4.50E-06
v01	2.00E-07	1.14E-05	4.50E-04	4.50E-06
v02	1.00E-06	1.14E-05	3.50E-04	4.50E-06
v03	4.00E-05	1.14E-05	1.00E-04	4.50E-06
v04	2.00E-06	1.14E-05	2.00E-04	4.50E-06
v05	1.00E-06	1.14E-05	2.50E-04	8.00E-06
v06	1.00E-06	5.00E-05	2.00E-04	4.50E-06
v07	**1.50E-06**	**3.00E-05**	**2.00E-04**	**4.50E-06**
v08	1.75E-06	4.00E-05	2.00E-04	4.50E-06

Table 3b. Aquitard Properties for Clay Cells by Calibration Iteration -- CCX				
Iteration	VK [ft/day]	Ss [1/ft]	Sfv [-]	Sfe [-]
v00	2.50E-05	1.14E-05	1.65E-04	4.50E-06
v01	2.00E-07	1.14E-05	4.50E-04	4.50E-06
v02	2.00E-05	1.14E-05	2.00E-04	4.50E-06
v03	2.50E-05	1.14E-05	1.00E-04	4.50E-06
v04	2.50E-05	5.00E-05	1.30E-04	4.50E-06
v05	**2.50E-05**	**3.00E-05**	**1.20E-04**	**4.50E-06**
v06	2.00E-04	3.00E-05	1.20E-04	8.00E-06
v07	2.00E-04	3.00E-05	1.50E-04	4.50E-06
v08	2.50E-04	3.00E-05	1.40E-04	4.50E-06
v09	2.00E-04	3.00E-05	1.40E-04	4.50E-06
v10	8.00E-05	3.00E-05	1.00E-04	4.50E-06

The calibration iterations with the best match between the simulated and observed values are highlighted in dark green.

Calibration iterations shown in Figures 4a-c are highlighted in light green.

Table 3c. Aquitard Properties for Clay Cells by Calibration Iteration -- APX				
Iteration	VK [ft/day]	Ss [1/ft]	Sfv [-]	Sfe [-]
v00	2.50E-05	1.14E-05	1.65E-04	4.50E-06
v01	2.00E-07	1.14E-05	4.50E-04	4.50E-06
v02	2.00E-06	1.14E-05	6.00E-04	4.50E-06
v03	2.00E-06	1.14E-05	2.00E-04	4.50E-06
v04	2.00E-06	1.14E-05	1.00E-04	4.50E-06
v05	2.00E-06	1.14E-05	8.00E-05	4.50E-06
v06	2.00E-06	1.14E-05	5.00E-05	4.50E-06
v07	2.00E-06	1.14E-05	3.00E-05	4.50E-06
v08	2.00E-06	1.14E-05	4.00E-05	4.50E-06
v09	2.00E-06	1.14E-05	4.75E-05	4.50E-06
v10	2.00E-05	2.00E-05	4.00E-05	4.50E-06
v11	2.00E-05	1.14E-05	5.00E-05	4.50E-06
v12	8.00E-06	1.14E-05	5.00E-05	4.50E-06
v13	1.00E-06	1.14E-05	5.00E-05	4.50E-06
v14	1.50E-06	1.14E-05	5.00E-05	4.50E-06
v15	1.75E-06		5.25E-05	4.50E-06
v16	1.50E-06	1.14E-05	4.75E-05	4.50E-06
v17	1.50E-06	8.00E-06	4.75E-05	4.50E-06
v18	1.75E-06	1.00E-05	5.25E-05	4.50E-06
v19	1.50E-06	9.00E-06	5.50E-05	4.50E-06
v20	1.30E-06	9.00E-06	4.50E-05	4.50E-06
v21	1.40E-06	1.00E-05	4.75E-05	4.70E-06
v22	1.55E-06	9.00E-06	5.50E-05	4.50E-06
v23	1.60E-06	9.25E-06	5.40E-05	4.60E-06
v24	1.58E-06	9.15E-06	5.30E-05	4.60E-06
v25	1.60E-06	9.20E-06	5.20E-05	4.60E-06
v26	1.55E-06	9.10E-06	5.25E-05	4.60E-06
v27	1.50E-06	9.00E-06	5.35E-05	4.55E-06
v28	1.50E-06	9.00E-06	5.35E-05	3.00E-06
v29	1.50E-06	9.00E-06	5.35E-05	3.00E-07
V30a	1.55E-06	8.50E-06	5.00E-05	3.00E-07
v30	1.55E-06	8.50E-06	4.00E-05	3.00E-07
v31	1.55E-06	8.50E-06	4.50E-05	3.00E-07
v32a	1.50E-06	8.50E-06	4.50E-05	3.00E-07
v32	1.25E-06	8.50E-06	4.50E-05	3.00E-07
33a	1.55E-06	9.00E-06	4.50E-05	3.00E-07
v33	**1.55E-06**	**5.00E-06**	**4.50E-05**	**3.00E-07**
34a	1.55E-06	5.00E-06	4.50E-05	1.65E-06
v34	1.55E-06	5.00E-06	4.50E-05	2.00E-06
v35	1.55E-06	5.00E-06	4.75E-05	2.00E-06

Table 4a. Calibration Statistics by Calibration Iteration -- ONT-33					
Iteration	Mean of Differences (Observed - Modeled) (ft)	Standard Deviation (ft)	Root Mean Square Deviation (RMSD) (ft)	R^2	NSE
V00	0.636	0.213	0.671	0.649	-5.767
V01	-0.9	0.352	0.966	0.991	-13.043
V02	-0.759	0.295	0.815	0.986	-8.975
V03	0.711	0.236	0.749	0.512	-7.426
V04	0.183	0.09	0.204	0.917	0.377
V05	-0.285	0.123	0.311	0.979	-0.453
V06	-0.076	0.057	0.095	0.979	0.863
V07	**0.037**	**0.054**	**0.066**	**0.956**	**0.935**
V08	0.074	0.061	0.096	0.948	0.861

Table 4b. Calibration Statistics by Calibration Iteration -- CCX					
Iteration	**Mean of Differences (Observed - Modeled) (ft)**	**Standard Deviation (ft)**	**Root Mean Square Deviation (RMSD) (ft)**	**R^2**	**NSE**
V00	-0.01	0.038	0.039	0.897	0.889
V01	-0.044	0.066	0.079	0.704	0.058
V02	-0.07	0.087	0.112	0.789	0.604
V03	0.026	0.032	0.041	0.816	0.695
V04	-0.002	0.032	0.032	0.905	0.904
V05	**0.009**	**0.027**	**0.028**	**0.914**	**0.905**
V06	0.046	0.044	0.063	0.627	0.21
V07	0.028	0.033	0.043	0.849	0.738
V08	0.014	0.04	0.042	0.853	0.829
V09	0.011	0.043	0.044	0.846	0.832
V10	0.014	0.027	0.031	0.899	0.871

Table 4c. Calibration Statistics by Calibration Iteration -- APX					
Iteration	Mean of Differences (Observed - Simulated) (ft)	Standard Deviation (ft)	Root Mean Square Deviation (RMSD) (ft)	R^2	NSE
V0	-3.079	4.024	5.067	0.176	-0.326
V1	-1.403	1.126	1.799	0.548	-0.171
V2	-5.613	5.896	8.14	0.275	-0.383
V3	-1.9	2.267	2.958	0.302	-0.193
V4	-0.662	0.939	1.148	0.444	0.163
V5	-0.377	0.627	0.732	0.556	0.392
V6	0.085	0.155	0.177	0.915	0.886
V7	0.419	0.328	0.532	0.642	-0.092
V8	0.249	0.163	0.298	0.899	0.601
V9	0.126	0.134	0.184	0.934	0.867
V10	-0.036	0.36	0.362	0.689	0.685
V11	-0.335	0.695	0.772	0.467	0.333
V12	-0.155	0.468	0.493	0.609	0.562
V13	0.179	0.104	0.207	0.961	0.807
V14	0.124	0.109	0.166	0.957	0.889
V15	0.064	0.157	0.17	0.915	0.899
V16	0.124	0.109	0.166	0.957	0.889
V17	0.109	0.118	0.161	0.949	0.899
V18	0.058	0.163	0.173	0.909	0.896
V19	0.038	0.165	0.169	0.91	0.904
V20	0.208	0.126	0.243	0.941	0.732
V21	0.171	0.108	0.202	0.958	0.823
V22	0.033	0.173	0.176	0.902	0.898
V23	0.047	0.166	0.173	0.907	0.898
V24	0.064	0.152	0.165	0.92	0.904
V25	0.078	0.143	0.163	0.928	0.903
V26	0.074	0.142	0.16	0.929	0.907
V27	0.062	0.147	0.159	0.925	0.91
V28	0.088	0.14	0.165	0.93	0.899
V29	-0.062	0.147	0.16	0.933	0.921
V30	0.137	0.126	0.186	0.935	0.846
V31	0.058	0.076	0.096	0.979	0.963
V32	0.091	0.086	0.125	0.972	0.933
V33	**0.033**	**0.076**	**0.083**	**0.979**	**0.973**
V34	0.089	0.086	0.124	0.974	0.938
V35	0.049	0.1	0.111	0.965	0.953